Suppression of Arctic sea ice growth by winter clouds and snowfall

Won-il Lim
Pusan National University
Hyo-Seok Park (hspark1@gmail.com)
Hanyang University https://orcid.org/0000-0002-2074-2656
Andrew Stewart
University of California, Los Angeles https://orcid.org/0000-0001-5861-4070
Kyong-Hwan Seo
Pusan National University

Article

Keywords: Arctic warming, snowfall, sea ice

Posted Date: January 18th, 2021

DOI: https://doi.org/10.21203/rs.3.rs-84779/v1

Suppression of Arctic sea ice growth by winter clouds and snowfall

Won-il Lim[1], Hyo-Seok Park[2*], Andrew L. Stewart[3] and Kyong-Hwan Seo[1]

[1]*Department of Atmospheric Sciences, Pusan National University, Busan, South Korea*

[2]*Department of Ocean Science and Technology, Hanyang University, Ansan, South Korea*

[3]*Department of Atmospheric and Oceanic Sciences, University of California, Los Angeles, USA*

Abstract

The ongoing Arctic warming has been pronounced in winter and has been associated with an increase in downward longwave radiation. While previous studies have demonstrated that poleward moisture flux into the Arctic strengthens downward longwave radiation, less attention has been given to the impact of the accompanying increase in snowfall. Here, utilizing state-of-the art sea ice models, we show that typical winter snowfall anomalies of 1.0 cm, accompanied by positive downward longwave radiation anomalies of ~5 W m^{-2} can decrease sea ice thickness by around 5 cm in the following spring over the Eurasian Seas. This basin-wide ice thinning is followed by a shrinking of summer ice extent in extreme cases. In the winter of 2016–17, anomalously strong warm/moist air transport combined with ~2.5 cm increase in snowfall decreased spring ice thickness by ~10 cm and decreased the following summer sea ice extent by 5–30%. Projected future reductions in the thickness of Arctic sea ice and snow will amplify the impact of anomalous winter snowfall events on winter sea ice growth and seasonal sea ice thickness.

Introduction

The multi-decadal retreat in Arctic sea ice has been superposed upon pronounced interannual variability, which has motivated efforts to understand year-to-variability in the winter sea ice growth season[1–3]. For example, previous studies have shown that the initial sea ice thickness in late autumn–early winter preconditions the heat conductivity of the sea ice, and thereby strongly influences sea ice growth through the winter[2,3]. Autumn-winter variations in poleward moisture also modulate winter sea ice growth via changes in downward longwave radiation[4,5], and are predicted to become increasingly influential during the coming decades[3]. This study considers an additional direct effect of interannual variations in moisture transport into the Arctic on sea ice growth: increased winter snowfall. Over the Eurasian Seas, such as the Laptev, East Siberian, and Chukchi Seas, snowfall makes up more than 60% of the annual precipitation[6]. Because the thermal conductivity of snow is about 7 times lower than ice, it may be expected to insulate the sea ice in these sectors from the atmosphere, and thus suppress winter ice growth[7,8]. This insulation should be particularly effective in the Eurasian Seas, where relatively thin first-year ice is becoming increasingly dominant[9]. This raises the possibility that a small increase in snowfall associated with atmospheric moisture flux convergence may suppress sea ice growth throughout the winter. While previous studies have pointed out the close linkage between poleward moisture flux into the Arctic and increased downward longwave radiation[4,5,10], relatively little attention has been given to the accompanying increase in snowfall and its potential suppression of sea ice growth.

In this study, the impact of winter snowfall on the wintertime seasonal cycle of sea ice thickness is investigated using a state-of-the-art sea ice model, the Los Alamos sea-ice model CICE version 6.0 (hereafter CICE6)[11]. The model is forced by an atmospheric state reconstructed

from the European Center for Medium-Range Weather Forecasts version 5 (ERA5) reanalysis dataset[12]. An interim version of ERA5, ERA-interim[13] has shown the best performance in simulating the Arctic surface radiative fluxes[14] and precipitation[15] among various reanalysis products. By performing idealized perturbations experiments using CICE6, we demonstrate that typical positive winter snowfall anomalies of 1.0 cm suppress the sea ice growth over the Eurasian Seas in the winter and early spring and cause substantial ice thinning in the following late spring and summer. We further demonstrate that the snowfall-driven sea ice thinning is doubled by the accompanying strengthening of downward radiation and that this combination is often sufficient to reduce summer sea ice extent.

Results

CICE6–slab ocean model simulation of sea ice thickness and extent

The satellite-observed August-September sea ice extent exhibits a rapid decline from 2001 to 2012, during which the sea ice extent has decreased by around 35% (black line of Fig. 1a). Our CICE6 simulation with ERA5 atmospheric boundary conditions simulates the observed variability and trend of summer sea ice extent well (blue line of Fig. 1a): the correlation coefficient between the August-September average sea ice extent in CICE6 and observations is 0.95. The seasonal cycles of sea ice extent and volume are also captured by CICE6 (Figs. 1c and 1d). Figure 1b shows that the CICE6-simulated interannual variations of the wintertime snow depth over sea ice, averaged over the entire Arctic, are well correlated with those of the coupled Pan-Arctic Ice-Ocean Modeling and Assimilation System (PIOMAS)[16] (the correlation coefficient is 0.73) and the NASA Eulerian Snow on Sea Ice Model (NESOSIM)[9].

However, the mean snow depth and the amplitude of the interannual variability simulated by PIOMAS and NESOSIM are about 30% larger than those of CICE6. Reconstruction of snow depth over Arctic sea ice is a challenging issue because in-situ observations of snow on sea ice have been sparse and the retrieval of snow depth from satellite measurements is still in the early stage[17]. Moreover, estimating the snow depth over the eastern Arctic is more difficult than other regions[18], probably because the eastern Arctic is mostly covered by first-year sea ice and snow depth is generally thinner than other regions[9].

Snow depth and ice growth rate in winter

To what extent is the wintertime sea ice growth controlled by snow? Snow is a relatively poor conductor of heat, compared with sea ice, because a substantial fraction of its volume is trapped air. In winter, the insulating effect of snow decreases the conductive heat flux $F_c{}^{\uparrow}$, through the sea ice and snow, and thus decreases the rate at which seawater freezes to the base of the sea ice.

The insulating effect of snow may be understood with the aid of a one-dimensional conceptual model of the sea ice/snow heat budget. Assuming that the sea ice is composed by a single homogeneous layer of ice for simplicity, and that the sea ice temperature instantaneously equilibrates to the heat fluxes at its base and to the atmospheric conditions above the ice and snow, the heat balance at the ice-atmosphere interface can be written as

$$F_c{}^{\uparrow} = F_{LW}{}^{\uparrow} - F_{LW}{}^{\downarrow} + SHF^{\uparrow} + LHF^{\uparrow}. \quad (1)$$

Here, $F_{LW}{}^{\uparrow}$ and $F_{LW}{}^{\downarrow}$ denote upward and downward longwave radiative fluxes, respectively, and $SHF^{\uparrow}$ and $LHF^{\uparrow}$ denote upward sensible and latent heat fluxes, respectively. We have

89 neglected net shortwave radiation $F_{SW}{}^{\downarrow} + F_{SW}{}^{\uparrow}$ which is much weaker than other heat fluxes
90 in winter. Increased snowfall suppresses the ice growth by reducing the upward conductive
91 heat flux ($F_c{}^{\uparrow}$), leading to a lower snow surface temperature and decreased sensible heat flux
92 ($SHF^{\uparrow}$) and upward longwave radiation ($F_{LW}{}^{\uparrow}$).

93 Following ref. [2], we examined the basin-scale sea ice growth rate from November, during which
94 the Arctic Ocean basin above is mostly covered by sea ice. Because the delayed freeze-up in
95 recent decades has substantially decreased sea ice cover, it is difficult to quantify the basin-
96 scale snowfall forcing on the first-year sea ice in October. Moreover, the sea ice growth rate is
97 more closely related to the late summer sea ice thickness than to the atmospheric state in
98 October[3].

99 In our CICE6 simulations, the interannual variability of the ice growth rate from November to
100 March is strongly correlated with snow depth in winter, when averaged over the entire Arctic
101 (Fig. 2a), consistent with our expectation that the decreased conductivity of the sea ice/snow
102 layer should suppress ice growth. However, the insulating effect of snow on sea ice is
103 geographically dependent. Over the Atlantic sector of the Arctic, the accumulated winter
104 snowfall often exceeds 25 cm (Fig. 3a) and snow-ice formation is generally larger than 50 cm
105 (Fig. 3b). Anomalously large winter snowfall over the Atlantic Seas tends to produce
106 anomalously thick ice, rather than anomalously thin ice[19,20]. In this study, we focus on the snow
107 effect on sea ice in *the Eurasian Seas*, where the first-year sea ice is becoming increasingly
108 dominant[9] and the snow-ice formation is relatively small. Over the Eurasian Seas, the
109 correlation coefficient between the areally-averaged *detrended* snow depth and the *detrended*
110 ice growth rate is –0.80 (Fig. 2b), indicating that the insulation effect of snow cover is probably
111 dominant over the snow-ice formation.

This statistical relationship between the wintertime snow depth and ice growth is consistent with a simple one-dimensional (1D) ice-snow model, indicated via red-dotted lines in Figs. 2a and 2b. This 1D model indicates that increasing the wintertime mean snow depth from 13 cm to 18 cm can suppress the ice growth rate by around 2 cm $month^{-1}$, or approximately 10 cm over a five-month period (NDJFM). The ice growth rate variations predicted by snow depth changes alone in this 1D model (red-dotted lines) generally underestimates the sensitivity estimated from the interannual relationship between snow depth and ice growth rate (green scatter plots), both when averaged over the entire Arctic and over the Eurasian Seas (Figs. 2a and 2b). In our CICE6 simulations, a 5 cm increase in snow depth suppresses the ice growth rate by around 4 cm $month^{-1}$ (green dots in Figs. 2a and 2b), i.e. approximately 20 cm over a five-month period (NDJFM). This suggests that there may be other factors that co-vary with snow depth (or snowfall) and suppress sea ice growth, as will be explored in the following sections.

To identify the spatial pattern of snow depth and ice growth rate on interannual time scales, we construct composite maps of snow depth and ice growth rate anomalies, as shown in Figs. 2c and 2d. In this study, we applied a simple linear regression analysis: the linear relationship between the winter snow depth anomaly and the ice growth from November to March is calculated. Specifically, the ice growth rate at each grid point is regressed on the winter (NDJFM) snow depth anomaly averaged over the *Eurasian Seas*, including the Laptev, East Siberian, and Chukchi Seas (60°E–240°E; 69°N–90°N). We then present the winter ice growth (cm) at each geographical location per *one standard deviation (1 s.d.)* of areally-averaged snow depth anomaly. Note that we removed the linear trend in the snow depth to define the anomalies. From this point on, we focus on the *Eurasian Seas*, where a relatively large fraction of sea ice

cover is composed of first-year ice[3] and snow-ice formation is small (Fig. 3b).

The regression map exhibits a basin-wide increase in snow depth (Fig. 2c) and a basin-wide decrease of the ice growth rate (Fig. 2d), corroborating our earlier finding of a link between snow depth and ice growth over the Eurasian sector of the Arctic. On sub-basin scales, however, the spatial pattern of the reduced ice growth (Fig. 2d) does not visibly correspond to that of the snow depth (Fig. 2c). This may be due to other factors, such as atmospheric circulations and wind-driven ice drift, that modify the spatial patterns of both snow depth and ice thickness. In order to overcome this limitation, we designed idealized experiments that modulate s*nowfall* in our sea ice model. Unlike snow depth, which is a diagnostic variable of the sea ice model, *snowfall* is unambiguously a forcing for ice thickness and is an input variable for our sea ice model. Over the first-year sea ice region, we define as locations where the October-average sea ice concentration is less than 15%, snow depth is generally controlled by snowfall (Supplementary Fig. 1). Specifically, the areally-averaged interannual correlation between the winter (NDJFM) snowfall accumulation and the snow depth is about 0.80 over the first-year sea ice region.

The impact of winter snowfall on seasonal sea ice thickness

To quantitatively assess the impact of anomalously large winter snowfall on sea ice, we performed idealized perturbation experiments using CICE6. Specifically, we imposed climatological-mean 6-hourly snowfall (the five-month (NDJFM) climatological mean snowfall is shown in Fig. 3a) in the model from November to March for each of the 39 winters in the simulated period. Because of the increasing trend of winter snowfall over the recent 40 years (Fig. 4a), we increased the snowfall climatology linearly from 1979-80 to 2017-18

158 following the linear regression line (red-dashed line in Fig. 4a for ERA5) for each month. It is
159 unclear whether the increasing winter snowfall trends in these reanalysis products are reliable
160 or not because in-situ observations of snow and snowfall on sea ice have been sparse in space
161 and time. In these experiments, the same historical atmospheric boundary conditions are used
162 to force the model. In summary, there are two experimental configurations: historical
163 atmospheric boundary conditions ($Hist_i$), and historical atmospheric boundary conditions with
164 climatological snowfall from November to March ($cSnow_i$). These model simulations have
165 been integrated through the winter and the following summer of each year and these two
166 simulation outputs are subtracted ($Hist_i$ – $cSnow_i$). The resulting differences quantify the
167 impact of the winter snowfall anomalies on the following seasonal cycle of sea ice thickness
168 and extent.

169 In Figures 4b–h, we plot 39-year regression maps, showing the model-simulated seasonal snow
170 depth (Figs. 4c–e) and sea ice thickness (Figs. 4f– h) responses to the winter snowfall anomalies
171 (Fig. 4b) on interannual time scales. Here, the winter accumulated snowfall, the seasonal snow
172 depth and the seasonal ice thickness anomalies at each grid point are regressed on the winter
173 accumulated snowfall anomaly averaged over the *Eurasian Seas*. The regression slopes are
174 multiplied by *one standard deviation of the snowfall anomaly* averaged over the *Eurasian Seas*,
175 which is approximately 1.0 cm in ERA5. The resulting snowfall map exhibits positive
176 anomalies over wide areas of the Eurasian Seas, especially over the Chukchi Sea and the Kara
177 Sea (Fig. 4b). A very similar pattern appears in other reanalysis datasets: the Japanese 55-year
178 reanalysis (JRA55)[21], the modern-era retrospective analysis for research and applications
179 version 2 (MERRA2)[22] and the climate forecast system reanalysis (CFSR)[23] (see
180 Supplementary Fig. 2). This geographic concentration may occur because a majority of Arctic

snowfall is associated with cyclone activity[24] and many of these cyclones pass through the Chukchi Sea and the Barents-Kara Seas. The snowfall in MERRA2 is about 20–25% larger than in the other reanalysis products (Fig. 4a) and using MERRA2 to force sea ice models is known to simulate thicker snow depth over sea ice[18]. Recent studies found that reanalysis products capture the satellite-observed and in-situ observed interannual variability in Arctic snowfall reasonably well [25,26].

Because of the snowfall accumulation throughout the winter, the snow depth anomalies peak in late winter and spring, from March to May (Fig. 4d). This regression map of ice thickness anomalies exhibits a basin-wide ice thinning throughout the winter and spring (Figs. 4f – h). The ice thickness anomaly is largest in the late winter and spring (Fig. 4g) and persists into the summer (Fig. 4h). From Fig. 4 we conclude that positive winter snowfall anomalies, which typically deviate from the climatology by 1.0 cm (*one standard deviation* of the winter snowfall averaged over the Eurasian Seas), suppress the winter ice growth and can cause basin-wide ice thinning through the following spring and summer. On the contrary, idealized experiments also indicate that anomalously large winter snowfall over *the Atlantic Seas*, defined as larger than one standard deviation on interannual time scales, rather causes ice thickening (Supplementary Fig. 3). As shown in previous studies[19,20], extreme snowfall events over the Atlantic sector of the Arctic substantially increase snow-ice formation and thereby can increase ice thickness.

Covariance between winter snowfall and downward longwave radiation

Because precipitation is dynamically tied to clouds and water vapor, the anomalously large wintertime snowfall is accompanied by stronger downward longwave radiation. On interannual time scales, the winter snowfall is strongly correlated with downward longwave radiation over

the Eurasian Seas and both exhibit increasing trends since early 2000's (Fig. 5a). In addition, downward longwave radiation is closely coupled to surface air temperature during the winter[10,27] and is often accompanied by surface air moistening. The interannual variabilities of 2m air temperature and near-surface specific humidity, averaged over the Eurasian Seas, are very similar each other (Fig. 5b), and are strongly correlated with those of snowfall / downward longwave radiation (compare Figs. 5a and 5b). The spatial patterns of snowfall (Fig. 5c), downward longwave radiation (Fig. 5f), 2m air temperature and near-surface specific humidity (Figs. 5d and 5e) anomalies are also similar to one another. Because precipitation and downward longwave radiation are strongly tied to clouds, it is not surprising to see that the spatial pattern of cloud liquid water anomaly (Fig. 5g) is also very similar to those of snowfall and downward longwave radiation.

The surface air warming is often associated with the development of low pressure with cyclonic circulation (Fig. 5h) via hydrostatic balance[28]. These air temperature and humidity anomalies are in fact directly linked to the poleward moisture flux anomalies: the development of south-westerlies over the Barents-Kara Seas and the Chukchi Sea (vectors in Fig. 5h) contributes to the increased poleward moisture flux that strengthens downward longwave radiation[5,10], and likely increases precipitation (snowfall) over the Eurasian Seas as well.

The net effect of increased snowfall and the accompanying atmospheric forcings

To quantitatively assess the combined impact of snowfall, longwave radiation, air temperature and humidity anomalies on sea ice, we performed additional idealized perturbation experiments for all of the 39 winters in our sea ice model simulation. Similar to the cSnow experiments described above, we created a model configuration in which the NDJFM downward longwave

227 radiation, surface air temperature, specific humidity and snowfall are replaced by their
228 respective climatological means. We refer to this idealized experiment as
229 “cSnow+cDLW+cT+cq”. The combined impact of the increased snowfall, stronger downward
230 longwave radiation and the associated surface air warming/moistening can be estimated from
231 the difference between the historical simulation and the idealized experiment, Hist –
232 (cSnow+cDLW+cT+cq). Here the climatological mean values of downward longwave
233 radiation, surface air temperature and specific humidity are defined via linear regression lines,
234 shown in Figs. 5a and 5b.

235 The response of seasonal snow depth anomalies (Figs. 6a – c) to the combined forcings are
236 very similar to those of the snowfall forcing alone (Fig. 4c – e), which we attribute to the
237 surface air moistening keeping the surface relative humidity and the associated snow
238 sublimation almost unchanged. With the snow depth approximately unchanged, the increased
239 downward longwave radiation and surface air warming serve to further decrease the ice
240 thickness. Consequently, the sea ice thickness anomalies show a larger thinning (Fig. 6d) than
241 the snowfall forcing alone (Fig. 4f) in Dec-Jan-Feb. The suppression of winter ice growth is
242 followed by the ice thinning in the ensuing spring and summer. In Mar-Apr-May, sea ice
243 thickness decreases by around 4–8 cm (Fig. 6e), doubling the ice thickness anomalies driven
244 by the snowfall anomalies alone (compare Figs. 6e and 4g). The spatial patterns of the ice
245 thickness anomalies exhibit a pronounced ice thinning throughout the season, not only over the
246 Eurasian Seas, but also over the entire Arctic (Figs. 6d – f), and the majority these ice thickness
247 anomalies are statistically significant, exceeding 95% confidence interval derived from the
248 interannual ice thickness variations (stipples).

249 Because the basin-wide ice thinning persists into the summer (Fig. 6f), the summer sea ice

extent is likely to be affected. Indeed, our model simulates a non-negligible dependence of the summer sea ice extent on the preceding winter's snowfall and downward longwave radiation anomalies. Several years exhibited a notable reduction of the summer sea ice extent, particularly in recent years, during which the sea ice thinning might have increased the sensitivity of ice thickness to winter clouds and snowfall. In the winter of 2016–17, warm and moist air transported from lower latitudes by atmospheric rivers caused unprecedently warm Arctic, suppressing sea ice growth[5]. The wintertime snowfall was also large in the winter of 2016–17 not only over the Eurasian Seas but also over the wide areas of the Arctic, including the Barents and Kara Seas (Figs. 7a and 7d). CICE6 simulations show that the large snowfall combined with positive downward longwave and air temperature anomalies in the winter of 2016–17 suppressed the winter sea ice growth and decreased the spring and early summer sea ice thickness by ~10 cm over the Eurasian Seas (Fig. 7b). This seasonally persistent ice thinning was followed by a notable reduction of ice cover in August–September (Fig. 7c), which is approximately 30% reduction in sea ice extent.

Similarly, our CICE6 simulations also indicate that anomalously small snowfall and weak downward longwave radiation during the winter of 1998–99 (Figs. 8a and 8d) accelerated the winter sea ice growth and increased the spring and summer sea ice thickness up to 17 cm (Fig. 8b). This was followed by a large increase in summer sea ice concentration – more than 15% over wide areas of the Arctic Ocean in August–September (Fig. 8c). These results are consistent with previous studies[10,29,30] finding that downward longwave radiation anomalies in the Eurasian Seas precondition sea ice thickness, which in turn has nontrivial influence on summer sea ice extent. This study further presents that the accompanying increase in snowfall can double the ice thinning and thereby suggests that winter snowfall should be factored into

quantifying the impact of winter snowfall on seasonal sea ice thickness.

Sea ice model coupled to a full ocean model

A caveat of our modeling approach, CICE6 coupled to a slab ocean model, is that the ocean mixed layer depth cannot respond to changes in snowfall and downward longwave radiation. Such changes in the ocean mixed layer could feed back on sea ice growth, and so excluding them in CICE6 might bias our results. To test the robustness of our CICE6–slab ocean model simulations, we utilized the Community Earth System Model version 2 (CESM2)[31] forced by JRA55 atmospheric boundary conditions, which is one of the standard component sets.

The interannual variability of winter snowfall over the Eurasian Seas in JRA55 is very similar to that of ERA5 (Fig. 4a), except that the wintertime mean snowfall is about 10% smaller than that of ERA5. While using a full ocean model has merit in realistically simulating the interaction between sea ice growth/melting and the ocean mixed layer, it is difficult to control the SSTs over the marginal seas of the Arctic, which strongly influence sea ice extent[32]. Consequently, CESM2 forced by JRA55 atmospheric boundary conditions underestimates the summer sea ice extent by 10% (Supplementary Fig. 4).

Using CESM2 with JRA55 atmospheric boundary conditions, we performed the same perturbation experiments for the two extreme cases: the winters of 1998–99 and 2016–17. Consistent with the CICE6–slab ocean model simulations, CESM2 simulations show that the anomalously large snowfall (Fig. 7d), combined with other thermodynamic forcings, during the winter of 2016–17 suppressed the winter sea ice growth and decreased the spring and early summer sea ice thickness by ~10 cm (Fig. 7e). These sea ice thickness anomalies are similar to

295 those simulated in our CICE6–slab ocean model (compare Figs. 7b and 7e). This seasonally
296 persistent ice thinning is followed by a reduction of ice cover in August and September (Fig.
297 7f), which is approximately 5% reduction in sea ice extent. Note that direct comparisons of
298 summer sea ice concentration anomalies between the CICE6–slab ocean model and CESM2–
299 full ocean model outputs should be interpreted carefully because different atmospheric
300 boundary conditions are used (ERA5 vs. JRA55) and the CESM2–full ocean model simulates
301 a ~10% smaller summer sea ice extent than is simulated by the CICE6–slab ocean model
302 (compare Fig. 1a and Supplementary Fig. 4).

303 Consistent with our CICE6–slab ocean model simulations, the anomalously small snowfall and
304 weak downward longwave radiation during the winter of 1998–99 substantially increased sea
305 ice thickness throughout the seasons (Fig. 8e). The sea ice thickening was followed by an
306 increase in sea ice concentration in the summer of 1999 over wide areas of the Arctic Ocean
307 (Fig. 8f). It can be concluded that the simulation results from the CESM2–full ocean model
308 with JRA55 atmospheric boundary conditions generally corroborate those of the CICE6–slab
309 ocean model with ERA5 atmospheric boundary conditions.

310

311 ## Summary and discussion

312 In summary, our model simulations demonstrate that the Arctic winter snowfall serves as one
313 of the key controls of winter sea ice growth. A key finding of this study is that the effect of
314 winter snowfall on winter and spring sea ice thickness is comparable to that of downward
315 longwave radiation combined with surface air warming/moistening. The combined impacts on
316 sea ice are not limited to winter, but rather persist through the ensuing spring and summer. In

317 extreme cases, the basin-wide ice thinning is followed by a shrinking of summer ice extent.
318 This indicates that winter snowfall anomalies, along with accompanying anomalies in
319 downward longwave radiation and surface air warming/moistening, may serve as a useful
320 predictor of the following summer sea ice extent.

321 Arctic sea ice is projected to become thinner with future climate change, and snow depth is
322 likely to decline continuously[33,34]. As the idealized 1D model demonstrates, snow can be more
323 effective in suppressing the winter sea ice growth when the snow depth and sea ice thickness
324 are relatively thin (Fig. 9), suggesting that snowfall will more strongly influence the seasonal
325 sea ice growth and thickness in coming decades. This effect will be compounded by the
326 tendency for a warmer Arctic to be accompanied by increasing winter snowfall and decreasing
327 spring-summer snowfall (a majority of spring-summer snowfall becomes rainfall)[35] in the
328 coming decades. By the end of the 21st century, the autumn freeze-up of sea ice and the
329 associated snowfall accumulation are likely to be delayed by about 2~3 months[33], possibly
330 weakening the influence of the early winter snowfall on sea ice. Until then, the winter snowfall
331 and the accompanying atmospheric forcings are likely to be increasingly influential. As noted
332 in a recent study[3], the Arctic may be already transitioning to a state where the sea ice growth is
333 more controlled by the autumn-winter atmosphere/ocean forcing variations than the autumn
334 sea ice thickness.

335

336

337

338

Methods

1. Sea ice–slab ocean model configuration

To investigate the impact of snowfall on the seasonal ice thickness, we utilized a state-of-the-art model, the Los Alamos sea-ice model CICE version 6.0[11]. The material and thermal characteristics of sea ice are represented using an elastic-anisotropic-plastic rheology[36] and using mushy layer thermodynamics[37], respectively. The model has five ice categories with seven vertical layers and calculates energy fluxes between snow and each ice category. We use a displaced pole grid with 320×384 grid points, corresponding to a horizontal grid spacing of approximately 1 degree. Solar radiation over the sea ice is prescribed via the delta-Eddington method[38].

The sea ice model is coupled to a slab ocean model to simplify the ocean dynamics. The mixed layer depth in the Arctic Ocean has a seasonal cycle, ranging from depths greater than 20 m in winter to depths of 5–30 m in summer[39,40]. In this study, we imposed a spatially-uniform and seasonally-varying mixed layer depth based on the CMCC Global Ocean Physical Reanalysis System (C-GLORS) version 5[41], a global ocean reanalysis combined with in situ and satellite observations. We slightly reduced the C-CLORS mixed layer depth in summer to better track hydrographic observations (see Supplementary Fig. 5).

Over the sub-Arctic seas, where sea ice concentration is generally less than 15% throughout the season (since year 2000), we restored the sea surface temperatures to monthly historical SSTs. The rationale for this restoring is that the marginal seas, especially the Nordic Sea surface temperatures, have continuously increased over the last decades (Supplementary Fig. 6), and the slab ocean model of CICE6 underestimates this warming trend if the model is integrated

without the restoring. Other than imposing the SSTs in the marginal seas, we used default parameter values for the slab ocean, with zero 'deep ocean heat flux' (qdp=0). The sea surface salinity (SSS) is set to 31 PSU throughout the year, which is close to the observed salinity over the Arctic Ocean[42]. Thus, the modeled sea surface salinity does not respond to changes in ice growth and melt.

Historical simulation (Hist): Our simulations run for 40 years, from 1979 to 2018, during which satellite-observed Arctic sea ice concentration and reanalysis data are available. For the atmospheric forcing of CICE6, we utilized ERA5[12]. Specifically, we imposed 6-hourly meteorological fields (temperature, specific humidity, and zonal and meridional winds), 6-hourly radiative fluxes (downward shortwave and longwave radiation at the surface), and 6-hourly precipitation (rainfall and snowfall) in each model grid cell. CICE6 was integrated over 80 years to "spin up", during which we repeated the 1979–1988 atmospheric forcing eight times. The historical simulations were then initialized from the end of this spin-up simulation, starting from year 1979.

Validation: In order to validate the interannual variations of winter snowfall of ERA5, we examined the Japanese 55-year reanalysis (JRA55)[21], the modern-era retrospective analysis for research and applications version 2 (MERRA2)[22], and the climate forecast system reanalysis (CFSR)[23]. We found that these four reanalysis datasets exhibit consistent interannual variabilities (Fig. 4a and Supplementary Fig. 2). To validate the CICE6-simulated sea ice extent, we utilized the satellite-observed sea ice extent provided by the National Snow and Ice Data Center (NSIDC)[43]. To validate ice thickness and snow depth, we examined the coupled Pan-Arctic Ice-Ocean Modeling and Assimilation System (PIOMAS)[16] and the NASA Eulerian Snow on Sea Ice Model (NESOSIM)[9]. While PIOMAS spans 1979–present, NESOSIM spans

2000–2015.

Idealized perturbation experiments

(1) **Climatological winter snowfall experiment (cSnow)**: To identify the impact of anomalous snowfall on Arctic sea ice growth, we configured a CICE6 simulation in which the winter (November to March) snowfall in each year was replaced by climatological snowfall. The snowfall climatology is defined via the linear regression line of the winter snowfall averaged over the Eurasian Seas (red-dashed line in Fig. 4a). We then compared winter ice thicknesses between this simulation and our historical simulation to quantify the impact of anomalous snowfall. These idealized experiments were conducted until the following October to identify the impact of the winter snowfall on the subsequent spring and summer sea ice.

(2) Combination of parameters: the net effect of increased snowfall and accompanying atmospheric forcings (cSnow+cDLW+cT+cq): This experiment is designed to identify the combined effects of snowfall and downward longwave radiation, which is also accompanied by surface air warming and moistening. Similar to experiment cSnow, we configured CICE6 with historical atmospheric forcing, but replaced the downward longwave radiation, surface air temperature, surface specific humidity, and snowfall with their climatological counterparts from November to March in each year. We again integrated until the subsequent October of each year from 1979/80 to 2017/18. The climatological mean values of downward longwave radiation, surface air temperature and specific humidity are defined as linear regression lines, shown in Figs. 5a and 5b.

406 ## 2. CESM2: Sea ice–full ocean model simulations

407 To verify the robustness of CICE6–slab ocean model simulations, we also performed an ocean–
408 ice couple model experiment using the Community Earth System Model version 2 (CESM2)[31].
409 The ocean component of CESM2 is the second version of the Parallel Ocean Program (POP2)[44]
410 and Community Ice Code version 5 (CICE5)[45]. POP2 has a displaced North Pole horizontal
411 grid with gx1v7 grid resolution, which is the same as the CICE6–slab ocean used in this study,
412 and 60 vertical levels whose thicknesses monotonically increase from 10 m in the upper ocean
413 to 250 m in the deep ocean. The ocean-ice coupled model simulation is forced by a 3-hourly
414 atmospheric state (temperature, sea level pressure, humidity, winds), radiative fluxes
415 (downward longwave and shortwave), and precipitation from JRA55-do[46], a surface dataset
416 designed for driving ocean-sea ice models. The historical CESM2 ocean-sea ice simulations
417 driven by JRA55-do comprises one of the standard component sets of CESM2.

418 **Historical simulation (Hist)**: We integrated the model for 61 years from 1958 to 2018, then
419 used the first 21 years (from 1958 to 1978) as a spin-up simulation and the remaining 40 years
420 (from 1979 to 2018) as a historical simulation. Four different ensemble historical runs were
421 simulated by using 4 different initial conditions (perturbations in high latitude SSTs) of January
422 1979.

423 **Combination of parameters: the net effect of increased snowfall and accompanying**
424 **atmospheric forcings (cSnow+cDLW+cT+cq):** To identify the combined effects of snowfall
425 and downward longwave radiation, which is also accompanied by surface air warming and
426 moistening, we followed a similar procedure as in our CICE6–slab ocean model experiments.
427 We configured CESM2 with historical atmospheric forcing, but replaced the downward
428 longwave radiation, surface air temperature, surface specific humidity, and snowfall with their

429 climatological counterparts from November to March for 1998/99 and 2016/17. We again
430 integrated until the subsequent Octobers of 1999 and 2017, respectively. In each of these
431 experiments, we ran an ensemble of 4 simulations with SST perturbations. Each ensemble
432 member shows very similar sea ice thickness and concentration anomalies throughout the
433 season, probably because atmospheric boundary conditions are prescribed and the model is
434 integrated only for 12 months, from November to October. In this study, the ensemble means
435 of 2016/17 and 1998/99 are presented in Figs. 7 and 8, respectively.

436

437 **3. A simple one-dimensional (1D) sea ice model with snow**

438 To aid conceptual understanding of snow insulator effect on sea ice thickness, we construct a
439 minimal 1D column model of the Arctic snow/sea ice heat budget following ref. [47], assuming
440 a steady balance between upward conductive heat flux through the snow/ice layer and the net
441 surface heat loss. Utilizing bulk formulas for sensible and latent heat fluxes, equation (1) in the
442 main text can be re-written as:

443 $$F_c(T_S)^{\uparrow} = \sigma {T_S}^4 - {F_{LW}}^{\downarrow} + \rho_a c_p C_D \boldsymbol{U}(T_S - T_a) + \rho_a L_s C_D \boldsymbol{U}(q_{sat}(T_S) - q_a) \quad (2)$$

444 where T_S and T_a are snow-covered ice surface temperature and 2 m air temperature,
445 respectively. $\boldsymbol{U}$ is wind speed at 10 m and q_a is the specific air humidity at 2 m. q_{sat} is the
446 saturation specific humidity. σ is Stefan-Boltzmann constant and C_D is turbulent transfer
447 coefficient over sea ice.

448 Following ref. [48], which assumes a linear temperature gradient through snow and sea ice, the
449 conductive heat flux $F_c(T_S)^{\uparrow}$ is:

$$F_c(T_S)^{\uparrow} = \frac{k_i k_s (T_f - T_S)}{(k_i h_s + k_s h_i)} \qquad (3)$$

where T_f is the freezing temperature of sea water, h_i and h_s are thicknesses of ice and snow, respectively, and k_i and k_s are thermal conductivities of ice and snow, respectively. Note that snow is an effective thermal insulator: k_s is about seven times smaller than k_i. In winter, sea ice grows by conducting heat upward from the bottom of ice to the surface. Assuming that the ocean surface is at the freezing temperature, the freezing rate at the bottom of ice is simplified as:

$$\Phi_h = F_c^{\uparrow} / (\rho_i L_f) \qquad (4)$$

where ρ_i is density of ice and L_f is latent heat of fusion. Here, we calculate T_S and $F_c^{\uparrow}$ by solving equations (2) and (3) with prescribed thicknesses of ice and snow, h_i and h_s. Then, the ice growth rate Φ_h can be estimated from equation (4).

In this study, we estimated typical values of these parameters from ERA5, specifically wintertime (NDJFM) mean values over the Arctic Ocean averaged from 1979 to 2018. We used entire–Arctic averages for Fig. 2a and the Eurasian–sector averages for Fig. 2b. The parameters we used for the Eurasian sector of the Arctic Ocean are given below.

<u>Given parameters:</u>

c_p specific heat capacity of air, 1005 J kg^{-1} K^{-1}

C_D turbulent transfer coefficient over sea ice, 0.0013

k_i thermal conductivity of ice, 2.04 W m^{-1} K^{-1}

k_s thermal conductivity of snow, 0.31 W m^{-1} K^{-1}

L_f latent heat of fusion at 0 K , 3.340×10^5 J kg^{-1}

471 T_f freezing temperature of sea water, 271.3 K

472 ρ_i density of ice, 930 Kg m^{-3}

473 ρ_a density of air, 1.275 Kg m^{-3}

474 σ Stefan-Boltzmann constant, 5.67×10^{-8} W m^{-2} K^{-4}

475 $\boldsymbol{U}$ wind speed at 10 m, 2.56 $m\ s^{-1}$

476 h_i sea ice thickness, 1.38 m

477 T_a 2 m air temperature, 249.85 K

478 q_a 2 m specific humidity, 0.57 $g\ kg^{-1}$

479 ${F_{LW}}^{\downarrow}$ downward longwave radiation at the surface, 182.1 W m^{-2}

480

481 Because of its simplicity, the simple 1D model yields further physical insight into the effect of
482 snow depth on ice growth. The intuition is that thicker snow produces lower snow surface
483 temperature by decreasing the average conductivity of the snow/ice layer, which subsequently
484 decrease upward longwave radiation (${F_{LW}}^{\uparrow}$) and sensible heat flux ($SHF^{\uparrow}$).

485

486

487 **References**

488 1. Ricker, R. *et al.* Satellite-observed drop of Arctic sea ice growth in winter 2015–2016.
489 *Geophys. Res. Lett.* **44**, 3236–3245 (2017).

490 2. Stroeve, J. C., Schroder, D., Tsamados, M. & Feltham, D. Warm winter, thin ice?
491 *Cryosph.* **12**, 1791–1809 (2018).

492 3. Petty, A. A., Holland, M. M., Bailey, D. A. & Kurtz, N. T. Warm Arctic, Increased

493 Winter Sea Ice Growth? *Geophys. Res. Lett.* **45**, 12,922-12,930 (2018).

494 4. Woods, C., Caballero, R., Woods, C. & Caballero, R. The Role of Moist Intrusions in
495 Winter Arctic Warming and Sea Ice Decline. *J. Clim.* **29**, 4473–4485 (2016).

496 5. Hegyi, B. M. & Taylor, P. C. The Unprecedented 2016–2017 Arctic Sea Ice Growth
497 Season: The Crucial Role of Atmospheric Rivers and Longwave Fluxes. *Geophys. Res.*
498 *Lett.* **45**, 5204–5212 (2018).

499 6. Bintanja, R. & Andry, O. Towards a rain-dominated Arctic. *Nat. Clim. Chang.* **7**, 263–
500 267 (2017).

501 7. Sturm, M., Jon, H. & Perovich, D. K. Winter snow cover on the sea ice of the Arctic
502 Ocean at the Surface Heat Budget of the Arctic Ocean (SHEBA): Temporal evolution
503 and spatial variability. *J. Geophys. Res.* **107**, 8047 (2002).

504 8. Persson, P. O. G., Shupe, M. D., Perovich, D. & Solomon, A. Linking atmospheric
505 synoptic transport, cloud phase, surface energy fluxes, and sea-ice growth:
506 observations of midwinter SHEBA conditions. *Clim. Dyn.* **49**, 1341–1364 (2017).

507 9. Petty, A. A., Webster, M., Boisvert, L. & Markus, T. The NASA Eulerian Snow on
508 Sea Ice Model (NESOSIM) v1.0: initial model development and analysis. *Geosci.*
509 *Model Dev.* **11**, 4577–4602 (2018).

510 10. Park, H.-S., Lee, S., Kosaka, Y., Son, S.-W. & Kim, S.-W. The impact of arctic winter
511 infrared radiation on early summer sea ice. *J. Clim.* **28**, 6281–6296 (2015).

512 11. Craig, T. *et al.* CICE-Consortium/CICE: CICE version 6.0.0.,
513 https://doi.org/10.5281/ZENODO.1900639 (2018).

514 12. Copernicus Climate Change Service (C3S): ERA5: Fifth generation of ECMWF
515 atmospheric reanalyses of the global climate. Copernicus Climate Change Service
516 Climate Data Store (CDS), date of access,
517 https://cds.climate.copernicus.eu/cdsapp#!/home (2020).

518 13. Dee, D. P. *et al.* The ERA-Interim reanalysis: Configuration and performance of the
519 data assimilation system. *Q. J. R. Meteorol. Soc.* **137**, 553–597 (2011).

14. Zib, B. J. *et al.* Evaluation and Intercomparison of Cloud Fraction and Radiative Fluxes in Recent Reanalyses over the Arctic Using BSRN Surface Observations. *J. Clim.* **25**, 2291–2305 (2012).

15. Lindsay, R. *et al.* Evaluation of Seven Different Atmospheric Reanalysis Products in the Arctic. *J. Clim.* **27**, 2588–2606 (2014).

16. Zhang, J. & Rothrock, D. A. Modeling Global Sea Ice with a Thickness and Enthalpy Distribution Model in Generalized Curvilinear Coordinates. *Mon. Weather Rev.* **131**, 845–861 (2003).

17. Kwok, R., Kacimi, S., Webster, M. A., Kurtz, N. T. & Petty, A. A. Arctic Snow Depth and Sea Ice Thickness From ICESat-2 and CryoSat-2 Freeboards: A First Examination. *J. Geophys. Res. Ocean.* **125**, (2020).

18. Blanchard-Wrigglesworth, E., Webster, M. A., Farrell, S. L. & Bitz, C. M. Reconstruction of snow on arctic sea ice. *J. Geophys. Res. Ocean.* **123**, 3588–3602 (2018).

19. Granskog, M. A. *et al.* Snow contribution to first-year and second-year Arctic sea ice mass balance north of Svalbard. *J. Geophys. Res. Ocean.* **122**, 2539–2549 (2017).

20. Merkouriadi, I., Cheng, B., Graham, R. M., Rösel, A. & Granskog, M. A. Critical Role of Snow on Sea Ice Growth in the Atlantic Sector of the Arctic Ocean. *Geophys. Res. Lett.* **44**, 10479–10485 (2017).

21. Kobayashi, S. *et al.* The JRA-55 reanalysis: General specifications and basic characteristics. *J. Meteorol. Soc. Japan* **93**, 5–48 (2015).

22. Gelaro, R. *et al.* The modern-era retrospective analysis for research and applications, version 2 (MERRA-2). *J. Clim.* **30**, 5419–5454 (2017).

23. Saha, S. *et al.* The NCEP climate forecast system version 2. *J. Clim.* **27**, 2185–2208 (2014).

24. Webster, M. A., Parker, C., Boisvert, L. & Kwok, R. The role of cyclone activity in snow accumulation on Arctic sea ice. *Nat. Commun.* **10**, 5285 (2019).

25. Barrett, A. P., Stroeve, J. C. & Serreze, M. C. Arctic Ocean Precipitation From Atmospheric Reanalyses and Comparisons With North Pole Drifting Station Records. *J. Geophys. Res. Ocean.* **125**, (2020).

26. Cabaj, A., Kushner, P. J., Fletcher, C. G., Howell, S. & Petty, A. A. Constraining Reanalysis Snowfall Over the Arctic Ocean Using CloudSat Observations. *Geophys. Res. Lett.* **47**, (2020).

27. Woods, C., Caballero, R. & Svensson, G. Large-scale circulation associated with moisture intrusions into the Arctic during winter. *Geophys. Res. Lett.* **40**, 4717–4721 (2013).

28. Kim, K. Y. *et al.* Vertical Feedback Mechanism of Winter Arctic Amplification and Sea Ice Loss. *Sci. Rep.* **9**, (2019).

29. Liu, Y. & Key, J. R. Less winter cloud aids summer 2013 Arctic sea ice return from 2012 minimum. *Environ. Res. Lett.* **9**, 044002 (2014).

30. Letterly, A., Key, J. & Liu, Y. The influence of winter cloud on summer sea ice in the Arctic, 1983–2013. *J. Geophys. Res.* **121**, 2178–2187 (2016).

31. Danabasoglu, G. *et al.* The Community Earth System Model Version 2 (CESM2). *J. Adv. Model. Earth Syst.* **12**, (2020).

32. Bitz, C. M., Holland, M. M., Hunke, E. C. & Moritz, R. E. *Maintenance of the Sea-Ice Edge*. (2005).

33. Hezel, P. J., Zhang, X., Bitz, C. M., Kelly, B. P. & Massonnet, F. Projected decline in spring snow depth on Arctic sea ice caused by progressively later autumn open ocean freeze-up this century. *Geophys. Res. Lett.* **39**, (2012).

34. Webster, M. *et al.* Snow in the changing sea-ice systems. *Nature Climate Change* vol. 8 946–953 (2018).

35. Vihma, T. *et al.* The atmospheric role in the Arctic water cycle: A review on processes, past and future changes, and their impacts. *J. Geophys. Res. G Biogeosciences* **121**, 586–620 (2016).

36. Wilchinsky, A. V. & Feltham, D. L. Modelling the rheology of sea ice as a collection of diamond-shaped floes. *J. Nonnewton. Fluid Mech.* **138**, 22–32 (2006).

37. Feltham, D. L., Untersteiner, N., Wettlaufer, J. S. & Worster, M. G. Sea ice is a mushy layer. *Geophys. Res. Lett.* **33**, L14501 (2006).

38. Briegleb, B. P. & Light, B. *A Delta-Eddington Multiple Scattering Parameterization for Solar Radiation in the Sea Ice Component of the Community Climate System Model Tech. Note NCAR/TN-472+STR* (National Center for Atmospheric Research, 2007).

39. Cole, S. T., Timmermans, M. L., Toole, J. M., Krishfield, R. A. & Thwaites, F. T. Ekman veering, internal waves, and turbulence observed under arctic sea ice. *J. Phys. Oceanogr.* **44**, 1306–1328 (2014).

40. Peralta-Ferriz, C. & Woodgate, R. A. Seasonal and interannual variability of pan-Arctic surface mixed layer properties from 1979 to 2012 from hydrographic data, and the dominance of stratification for multiyear mixed layer depth shoaling. *Prog. Oceanogr.* **134**, 19–53 (2015).

41. Storto, A. & Masina, S. C-GLORSv5: An improved multipurpose global ocean eddy-permitting physical reanalysis. *Earth Syst. Sci. Data* **8**, 679–696 (2016).

42. Steele, M., Morley, R. & Ermold, W. PHC: A global ocean hydrography with a high-quality Arctic Ocean. *J. Clim.* **14**, (2001).

43. Fetterer, F., Knowles, K., Meier, W. N., Savoie, M. & Windnagel, A. K. *Sea ice index, version 3* (National Snow and Ice Data Center, 2017).

44. Smith, R. *et al.* The parallel ocean program (POP) reference manual: ocean component of the community climate system model (CCSM) and community earth system model (CESM). *Rep. LAUR-01853* 141, 1–140. (2010).

45. Hunke, E. C., Lipscomb, W. H., Turner, A. K., Jeffery, N. & Elliott, S. *CICE: the Los Alamos Sea Ice Model Documentation and Software User's Manual Version 5.1* LA-CC-06-012 (Los Alamos National Laboratory, Los Alamos, 2015).

46. Tsujino, H. *et al.* JRA-55 based surface dataset for driving ocean–sea-ice models (JRA55-do). *Ocean Model.* **130**, 79–139 (2018).

47. Petty, A. A., Feltham, D. L. & Holland, P. R. Impact of atmospheric forcing on Antarctic continental shelf water masses. *J. Phys. Oceanogr.* **43**, 920–940 (2013).

48. Semtner, A. J. A model for the thermodynamic growth of sea ice in numerical investigations of climate. *J. Phys. Oceanogr.* **6**, 379–389 (1976).

Correspondence to Hyo-Seok Park (hspark1@gmail.com)

Acknowledgement: HSP is supported by the National Research Foundation of Korea (NRF) no. 2020R1A2C2010025. ALS is supported by the National Sciences Foundation under grant number OCE-1751386.

Author Contributions: HSP initiated the project and WIL integrated CICE6 simulations. HSP and WIL carried out the analysis under the guidance of ALS and KHS. ALS developed the simple 1D sea ice model with snow cover. The manuscript was initially written by HSP and WIL, and was edited by ALS. All authors contributed to the interpretations of the results and the discussion of the manuscript.

Figure Legends

Fig. 1: Sea ice model simulation vs Observation

The year-to-year variations of **(a)** late summer (Aug–Sep) Arctic sea ice extent simulated by CICE (blue line) and from NSIDC observation (black line), and **(b)** the wintertime (NDJFM)

mean snow depth simulated by CICE (blue), PIOMAS (black) and NESOSIM (red). The climatological mean seasonal (monthly) variations of **(c)** sea ice extent and **(d)** sea ice volume. In **(c, d)**, blue shadings indicate the minimum/maximum ranges of sea ice extent and volume simulated by CICE, and gray shadings indicate the minimum/maximum ranges of **(c)** NSIDC observed sea ice extent and **(d)** PIOMAS sea ice volume.

Figure 2: Interannual relationship between snow depth and ice growth.

Interannual variation of the wintertime (NDJFM) mean snow depth (abscissa; cm) and ice growth rate (ordinate; cm $month^{-1}$) from 1979–80 to 2017–18 averaged over **(a)** the entire Arctic and **(b)** the Eurasian sector. The long-term trends of snow depth and ice growth rate have been removed. Red-dashed lines in **(a, b)** are from the 1D model calculation with fixed downward longwave radiation and surface air temperature (see Methods for details). The regression map of the wintertime **(c)** snow depth and **(d)** ice growth rate anomalies associated with area-averaged snow depth anomalies (per one standard deviation anomaly) in the Eurasian sector of the Arctic (red lines).

Fig. 3: Climatology and variability of snowfall and snow-ice formation

The wintertime (NDJFM) climatological mean **(a)** snowfall (cm), **(b)** snow-ice formation (cm), and one standard deviations of **(c)** snowfall (cm) and **(d)** snow-ice formation (cm) on interannual time scales. The long-term trends of snowfall and snow-ice formation have been removed. Snowfall and snow-ice formation are from ERA5 and CICE6 respectively.

Fig. 4: The impact of winter snowfall on seasonal ice thickness

(a) The interannual variations of wintertime (NDJFM) snowfall of ERA5, JRA55, MERRA2 and CFSR, averaged over the Eurasian sector (red line in **(b)**). The red-dashed line in **(a)** is a linear regression line for the winter snowfall in ERA5. **(b)** The regression map of snowfall anomalies in winter, per one standard deviation of winter snowfall anomaly over the Eurasian sector. The seasonal **(c, d, e)** snow depth and **(f, g, h)** sea ice thickness responses in **(c, f)** Dec–

Feb, **(d, g)** Mar–May, and **(e, h)** Jun–Aug to the anomalously large winter snowfall. In **(c)–(h)**, statistically significant values ($p < 0.05$) are stippled.

Fig. 5: Covariance between winter clouds, snowfall, and downward longwave radiation

The interannual variations of ERA5's wintertime (NDJFM) **(a)** snowfall (cm; red), downward longwave radiation (W m^{-1}; orange), **(b)** surface air temperature (K; black) and surface specific humidity (g kg^{-1}; blue) averaged over the Eurasian sector of the Arctic. The dotted lines are linear regression lines. The regression maps of **(c)** snowfall, **(d)** 2m air temperature, **(e)** near-surface specific humidity (g kg^{-1}), **(f)** downward longwave radiation, **(g)** cloud liquid water, and **(h)** sea level pressure (shadings, hPa) with winds (vectors, m s^{-1}) during the large snowfall winters (per one standard deviation of snowfall anomaly). The regression map of snowfall, **(c)** is identical to **Fig. 4b**.

Fig. 6: The net effect of the winter snowfall and accompanying atmospheric forcings on sea ice thickness

The seasonal **(a, b, c)** snow depth and **(d, e, f)** sea ice thickness responses in **(a, d)** Dec–Feb, **(b, e)** Mar–May, and **(c, f)** Jun–Aug to the anomalously large winter snowfall combined with strong downward longwave radiation, which is also accompanied by the surface air warming and moistening. Statistically significant values ($p < 0.05$) are stippled.

Fig. 7: 2016–17 sea ice responses simulated by CICE6–slab ocean and CESM2–full ocean models

(a, d) Snowfall anomalies during the winters of 2016-17 from ERA5 and JRA55, respectively. Simulated responses of **(b, e)** seasonal sea ice thickness and **(c, f)** summer (Aug-Sep) sea ice concentration to the combined effect of preceding winter snowfall and downward longwave radiation, which is also accompanied by the surface air warming and moistening. **(a)** is from ERA5 and **(d)** is from JRA55. **(b, c)** are derived from our CICE6–slab ocean experiments and **(e, f)** are derived from our CESM2–full ocean model simulations.

Fig. 8: **1998–99 sea ice responses simulated by CICE6–slab ocean and CESM2–full ocean models**

(a, d) Snowfall anomalies during the winters of 1998-99 and simulated responses of **(b, e)** seasonal sea ice thickness and **(c, f)** summer (Aug-Sep) sea ice concentration to the combined effect of preceding winter snowfall and downward longwave radiation, which is also accompanied by the surface air warming and moistening. **(a)** is from ERA5 and **(d)** is from JRA55. **(b, e)** are from our CICE6–slab ocean and **(c, f)** are from our CESM2–full ocean model simulations.

Figure 9: Sensitivity of ice growth rate to snow depth estimated by a simple 1D model

Sensitivity of wintertime ice growth rate (ordinate; cm month^{-1}) to snow depth (abscissa; cm) and ice thickness (red, black and blue lines), simulated by a simple 1D sea ice model. The red, black and blue lines correspond to sea ice thickness h_i = 1.0, 1.5 and 2.0 m respectively.

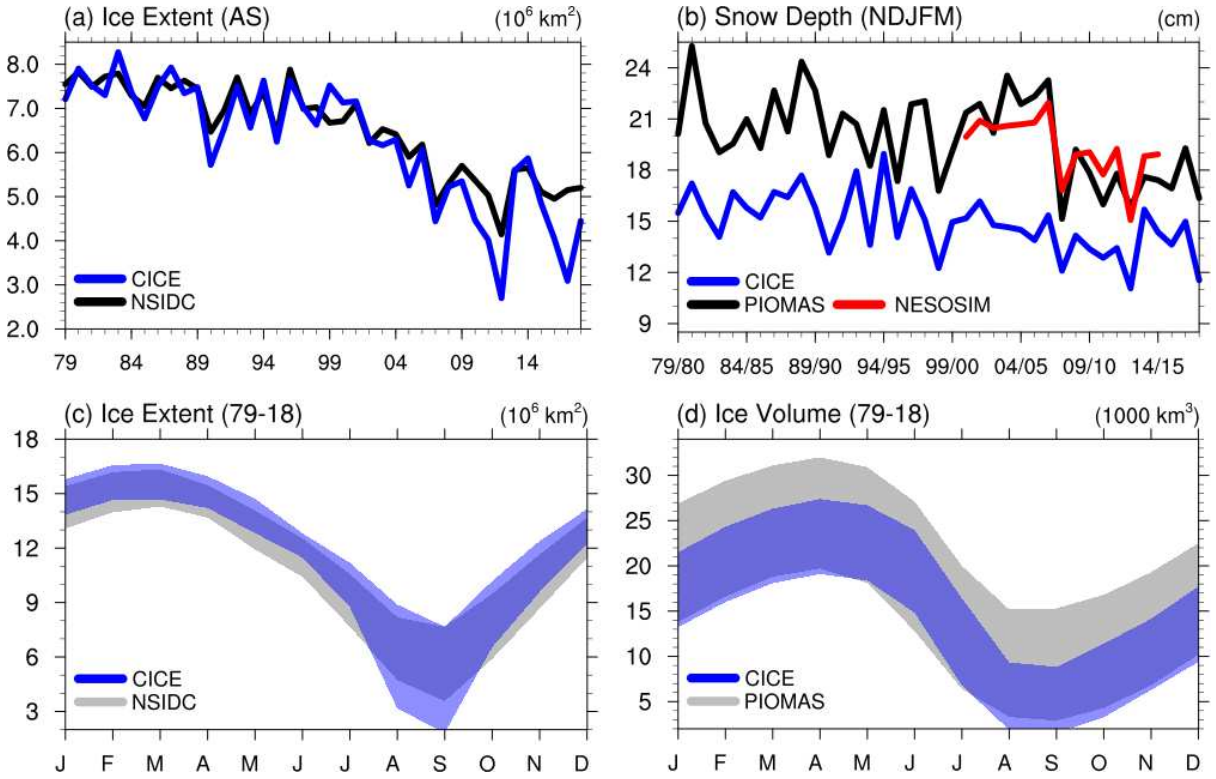

Fig. 1: Sea ice model simulation vs Observation

The year-to-year variations of **(a)** late summer (Aug–Sep) Arctic sea ice extent simulated by CICE (blue line) and from NSIDC observation (black line), and **(b)** the wintertime (NDJFM) mean snow depth simulated by CICE (blue), PIOMAS (black) and NESOSIM (red). The climatological mean seasonal (monthly) variations of **(c)** sea ice extent and **(d)** sea ice volume. In **(c, d)**, blue shadings indicate the minimum/maximum ranges of sea ice extent and volume simulated by CICE, and gray shadings indicate the minimum/maximum ranges of **(c)** NSIDC observed sea ice extent and **(d)** PIOMAS sea ice volume.

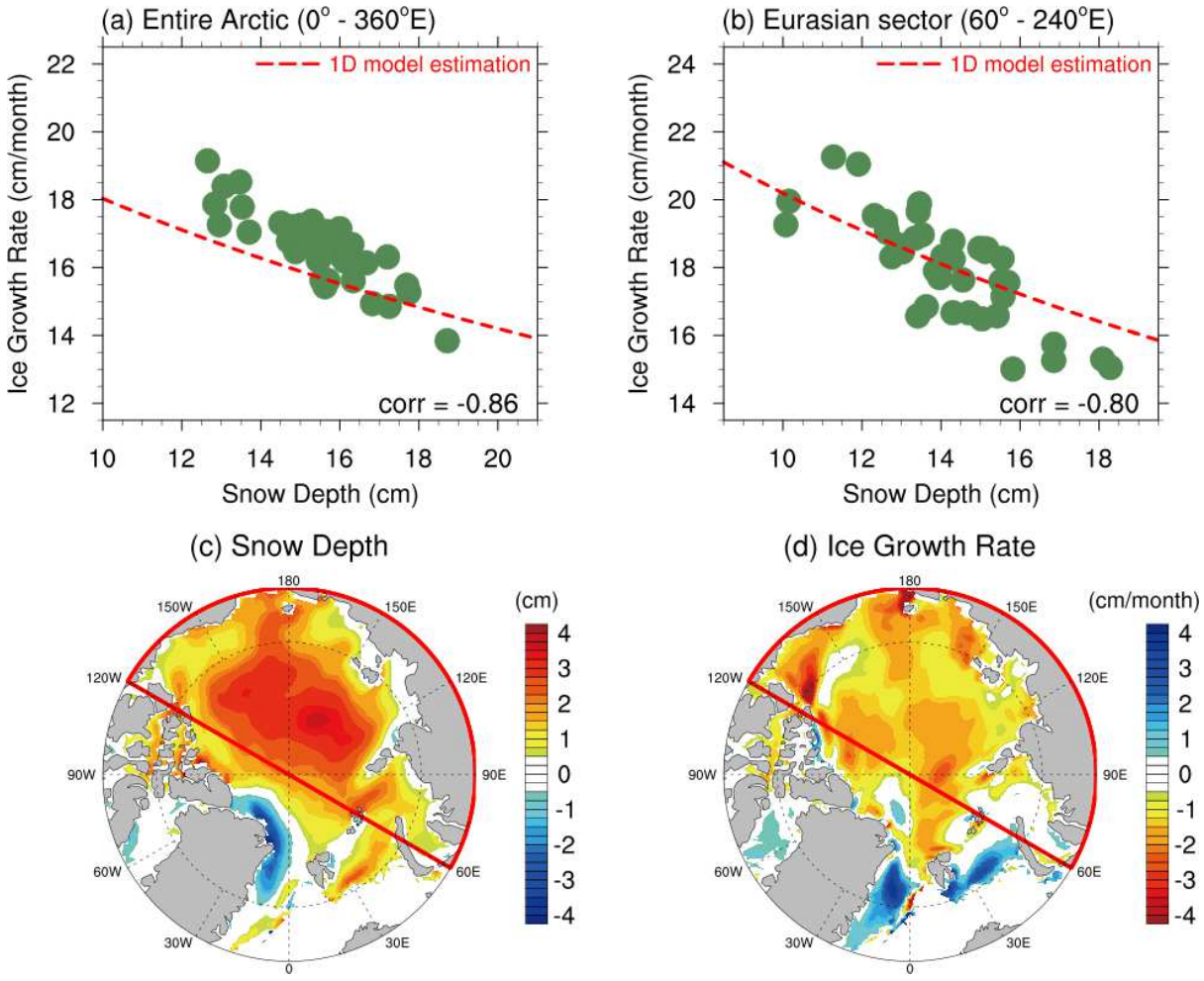

Figure 2: Interannual relationship between snow depth and ice growth.

Interannual variation of the wintertime (NDJFM) mean snow depth (abscissa; cm) and ice growth rate (ordinate; cm month^{-1}) from 1979–80 to 2017–18 averaged over **(a)** the entire Arctic and **(b)** the Eurasian sector. The long-term trends of snow depth and ice growth rate have been removed. Red-dashed lines in **(a, b)** are from the 1D model calculation with fixed downward longwave radiation and surface air temperature (see Methods for details). The regression map of the wintertime **(c)** snow depth and **(d)** ice growth rate anomalies associated with area-averaged snow depth anomalies (per one standard deviation anomaly) in the Eurasian sector of the Arctic (red lines).

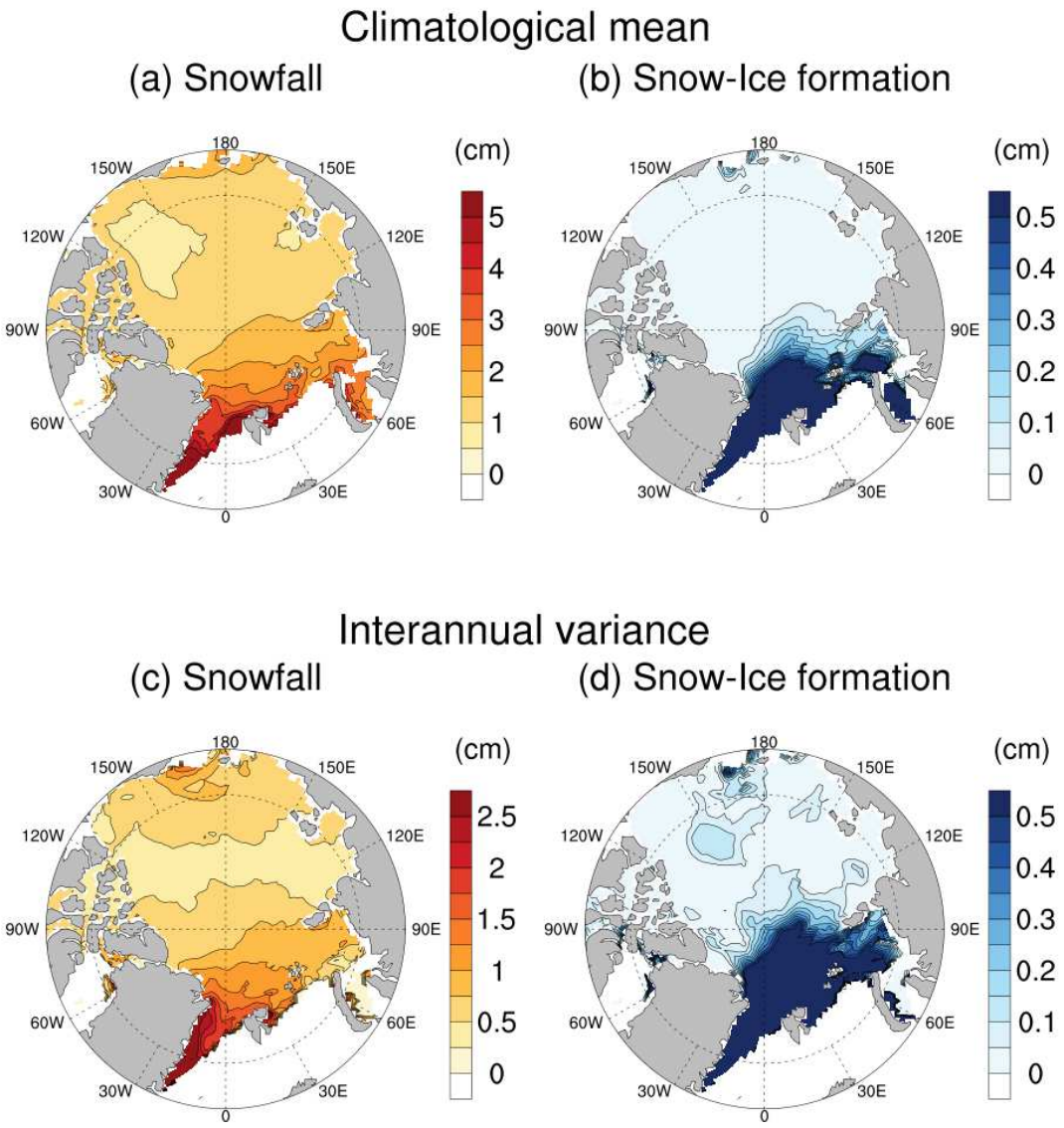

723

724

725 **Fig. 3: Climatology and variability of snowfall and snow-ice formation**

726 The wintertime (NDJFM) climatological mean **(a)** snowfall (cm), **(b)** snow-ice formation (cm),
727 and one standard deviations of **(c)** snowfall (cm) and **(d)** snow-ice formation (cm) on
728 interannual time scales. The long-term trends of snowfall and snow-ice formation have been
729 removed. Snowfall and snow-ice formation are from ERA5 and CICE6 respectively.

730

731

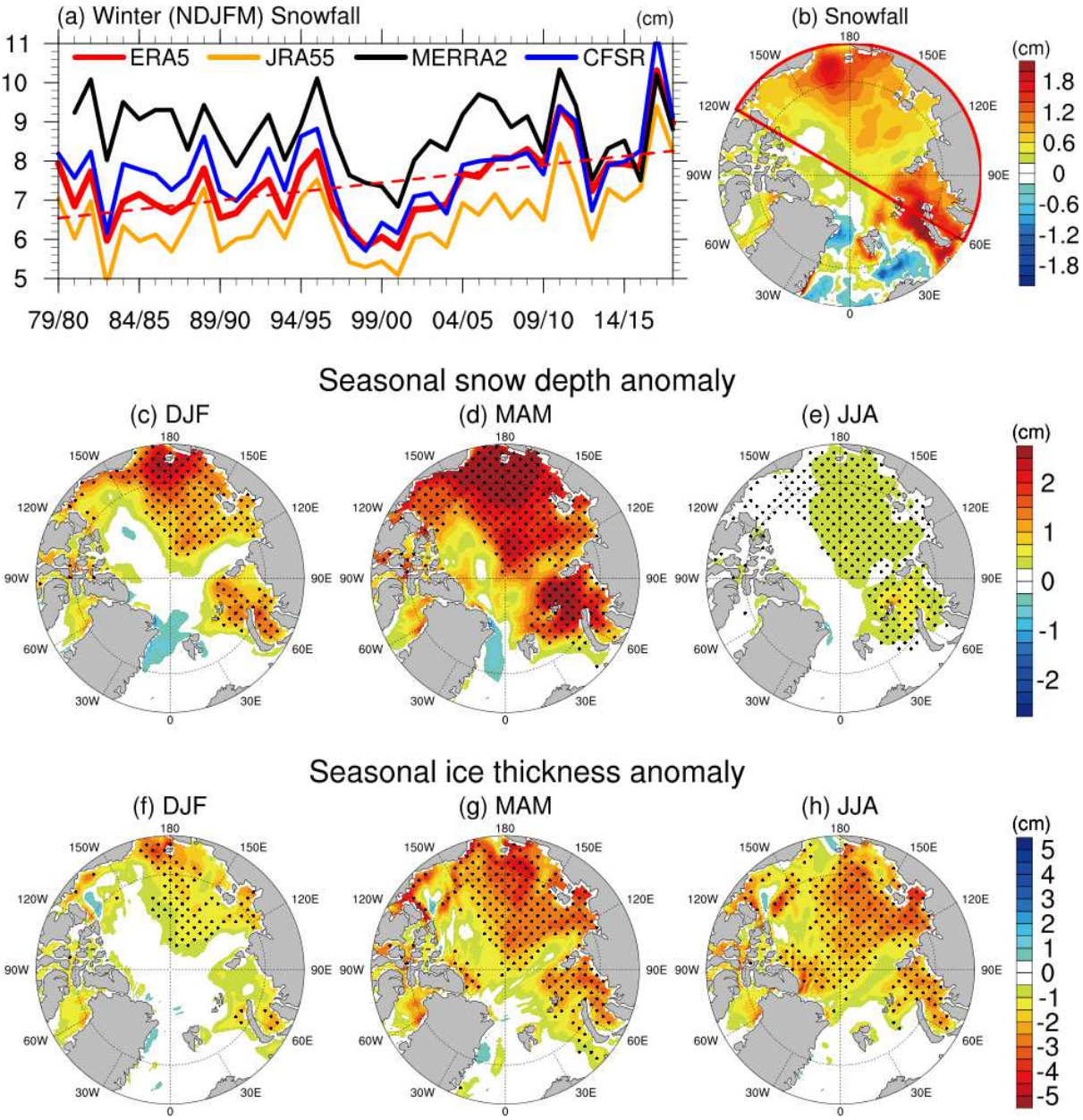

Fig. 4: The impact of winter snowfall on seasonal ice thickness

(a) The interannual variations of wintertime (NDJFM) snowfall of ERA5, JRA55, MERRA2 and CFSR, averaged over the Eurasian sector (red line in **(b)**). The red-dashed line in **(a)** is a linear regression line for the winter snowfall in ERA5. **(b)** The regression map of snowfall anomalies in winter, per one standard deviation of winter snowfall anomaly over the Eurasian sector. The seasonal **(c, d, e)** snow depth and **(f, g, h)** sea ice thickness responses in **(c, f)** Dec–Feb, **(d, g)** Mar–May, and **(e, h)** Jun–Aug to the anomalously large winter snowfall. In **(c)–(h)**, statistically significant values ($p < 0.05$) are stippled.

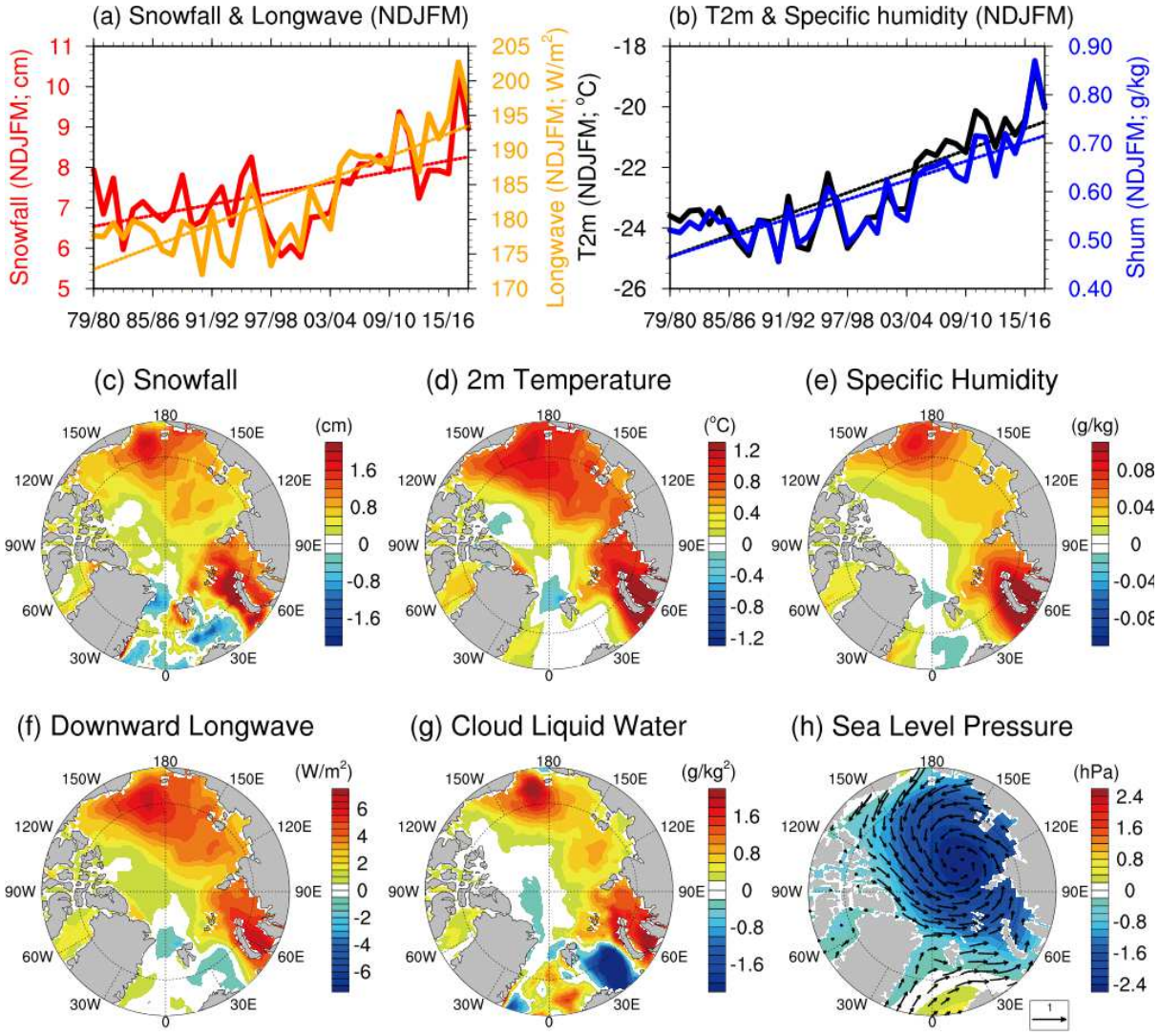

Fig. 5: Covariance between winter clouds, snowfall, and downward longwave radiation

The interannual variations of ERA5's wintertime (NDJFM) **(a)** snowfall (cm; red), downward longwave radiation (W m^{-1}; orange), **(b)** surface air temperature (K; black) and surface specific humidity (g kg^{-1}; blue) averaged over the Eurasian sector of the Arctic. The dotted lines are linear regression lines. The regression maps of **(c)** snowfall, **(d)** 2m air temperature, **(e)** near-surface specific humidity (g kg^{-1}), **(f)** downward longwave radiation, **(g)** cloud liquid water, and **(h)** sea level pressure (shadings, hPa) with winds (vectors, m s^{-1}) during the large snowfall winters (per one standard deviation of snowfall anomaly). The regression map of snowfall, **(c)** is identical to **Fig. 4b**.

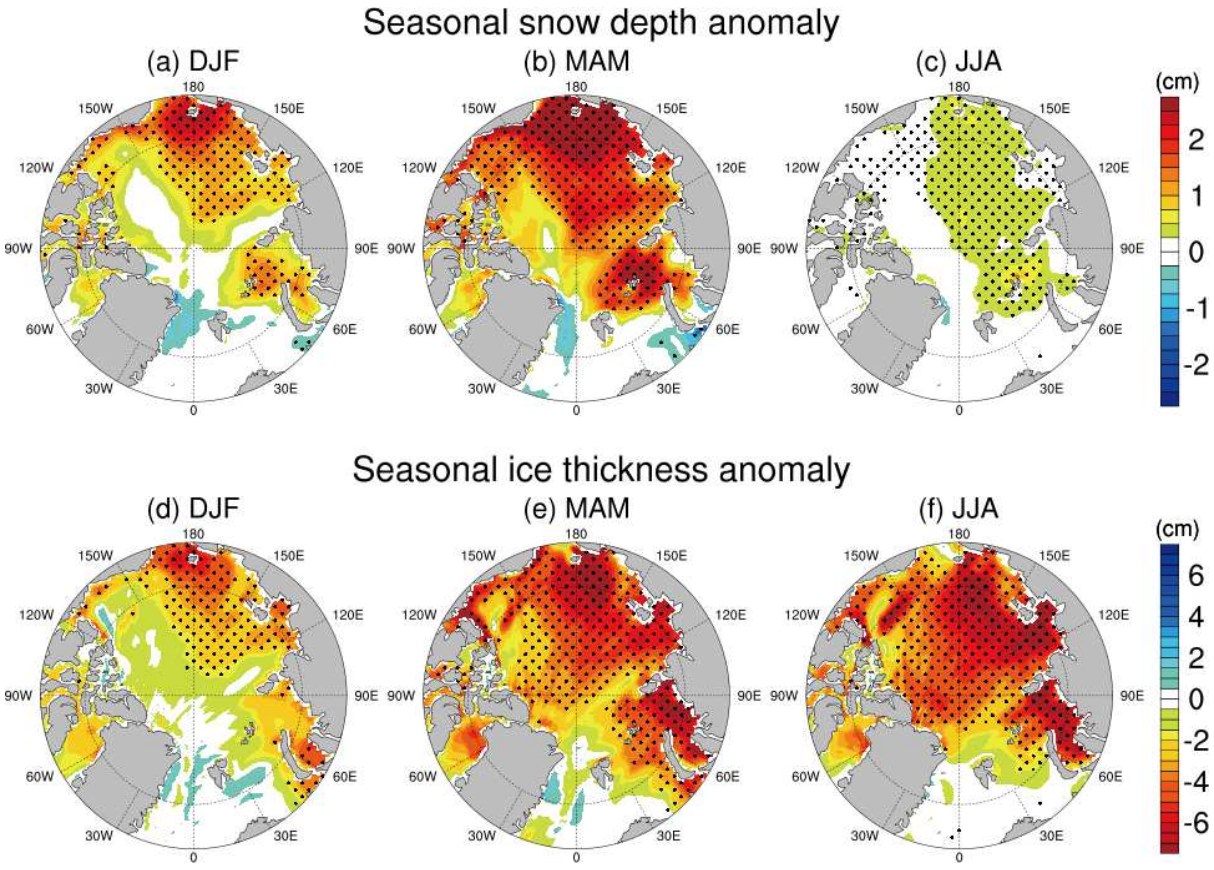

Fig. 6: The net effect of the winter snowfall and accompanying atmospheric forcings on sea ice thickness

The seasonal **(a, b, c)** snow depth and **(d, e, f)** sea ice thickness responses in **(a, d)** Dec–Feb, **(b, e)** Mar–May, and **(c, f)** Jun–Aug to the anomalously large winter snowfall combined with strong downward longwave radiation, which is also accompanied by the surface air warming and moistening. Statistically significant values ($p < 0.05$) are stippled.

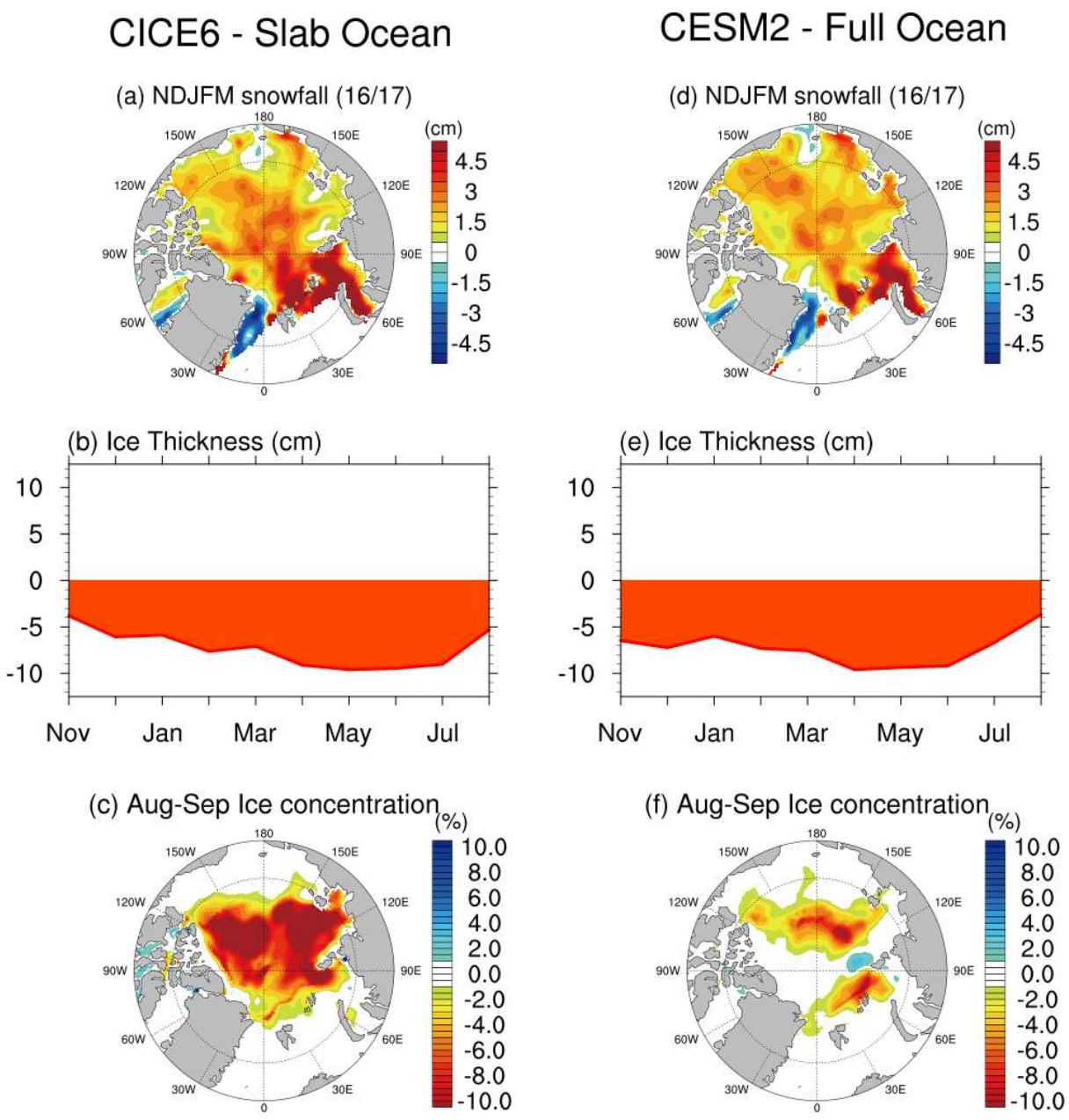

766

767

768 **Fig. 7: 2016–17 sea ice responses simulated by CICE6–slab ocean and CESM2–full ocean**
769 **models: (a, d)** Snowfall anomalies during the winters of 2016-17 from ERA5 and JRA55,
770 respectively. Simulated responses of **(b, e)** seasonal sea ice thickness and **(c, f)** summer (Aug-
771 Sep) sea ice concentration to the combined effect of preceding winter snowfall and downward
772 longwave radiation, which is also accompanied by the surface air warming and moistening. **(a)**
773 is from ERA5 and **(d)** is from JRA55. **(b, c)** are derived from our CICE6–slab ocean
774 experiments and **(e, f)** are derived from our CESM2–full ocean model simulations.

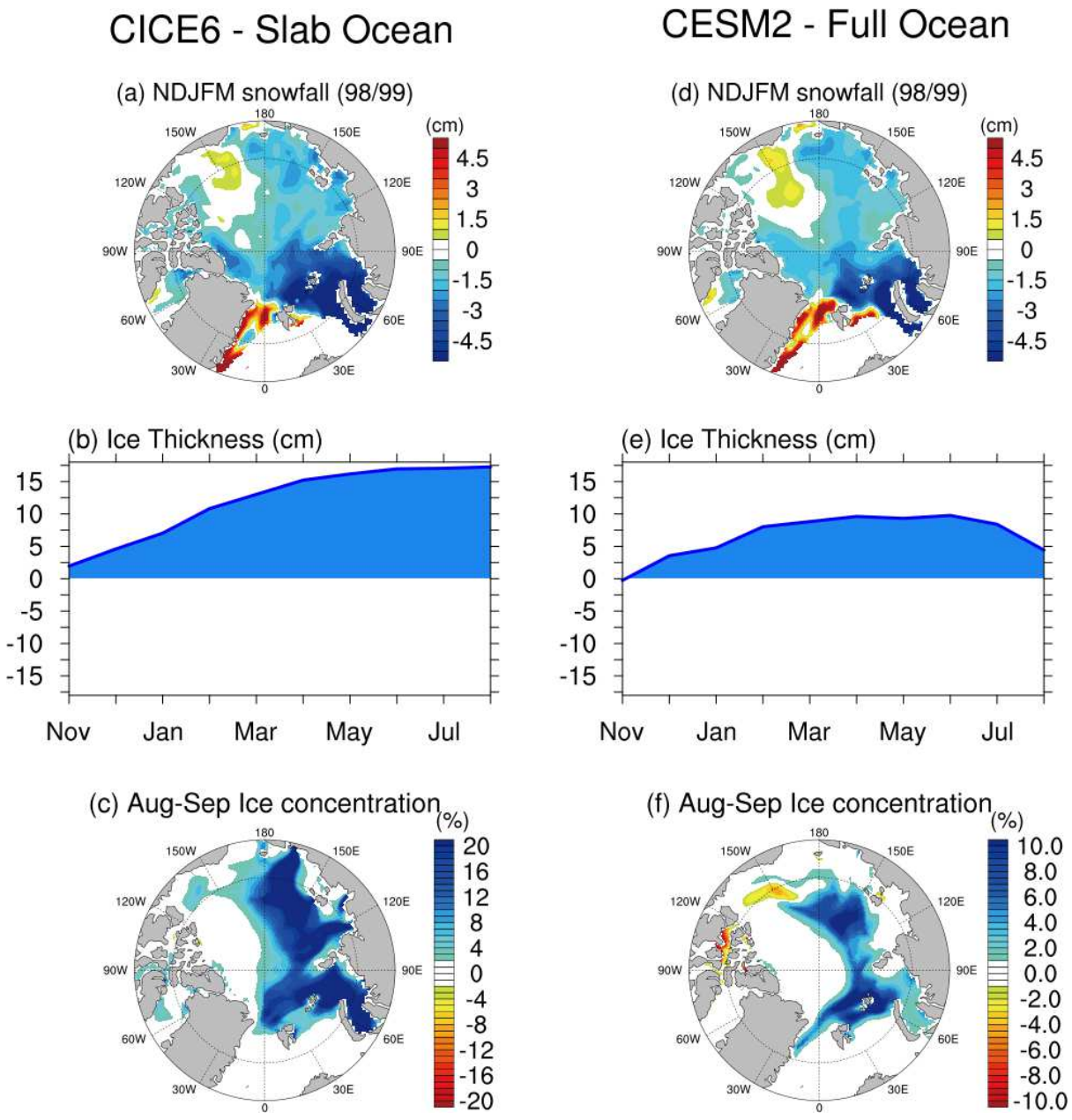

Fig. 8: **1998–99 sea ice responses simulated by CICE6–slab ocean and CESM2–full ocean models: (a, d)** Snowfall anomalies during the winters of 1998-99 and simulated responses of **(b, e)** seasonal sea ice thickness and **(c, f)** summer (Aug-Sep) sea ice concentration to the combined effect of preceding winter snowfall and downward longwave radiation, which is also accompanied by the surface air warming and moistening. **(a)** is from ERA5 and **(d)** is from JRA55. **(b, e)** are from our CICE6–slab ocean and **(c, f)** are from our CESM2–full ocean model simulations.

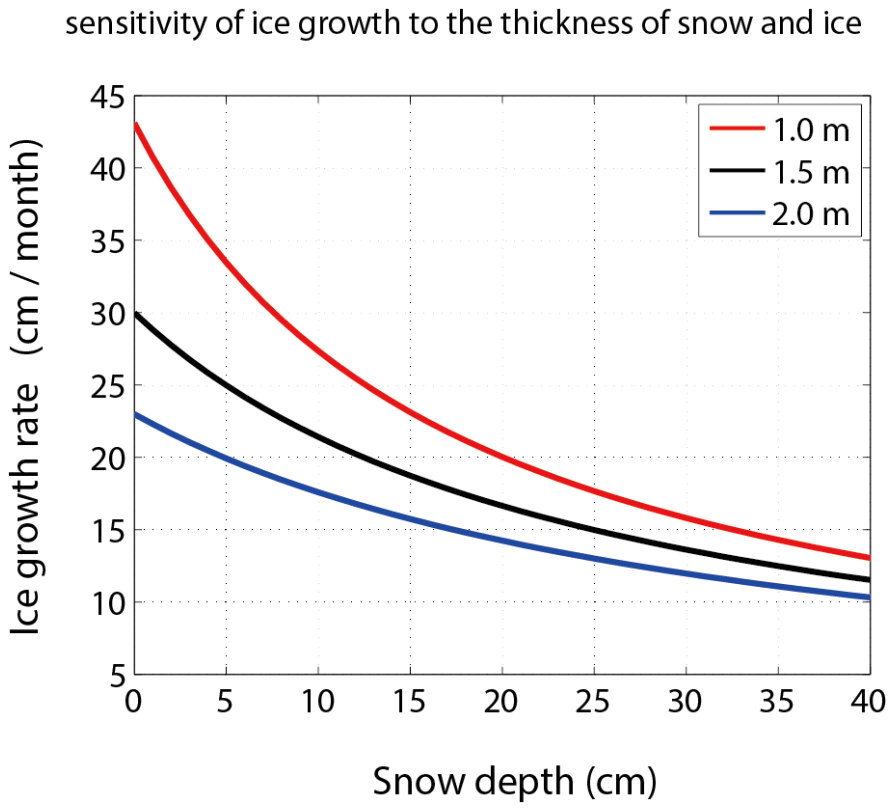

Figure 9: Sensitivity of ice growth rate to snow depth estimated by a simple 1D model

Sensitivity of wintertime ice growth rate (ordinate; cm month^{-1}) to snow depth (abscissa; cm) and ice thickness (red, black and blue lines), simulated by a simple 1D sea ice model. The red, black and blue lines correspond to sea ice thickness h_i = 1.0, 1.5 and 2.0 m respectively.

Figures

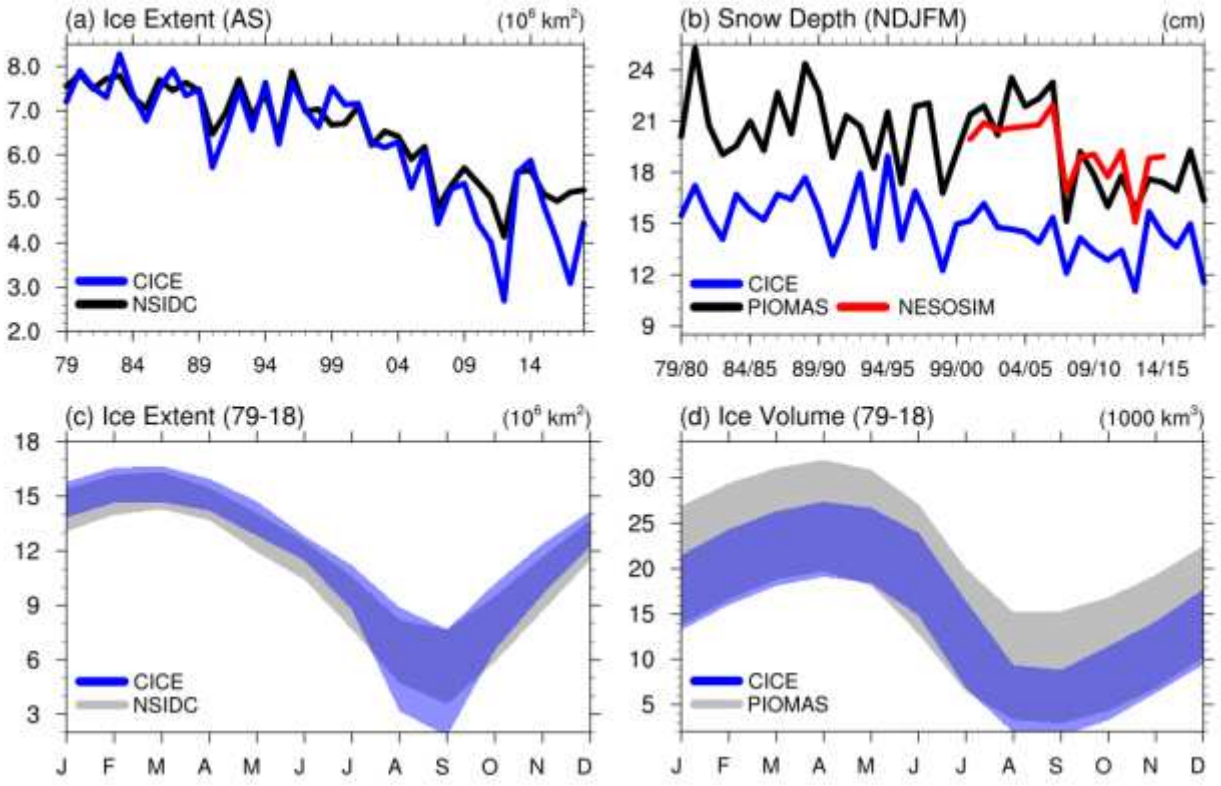

Figure 1

Sea ice model simulation vs Observation

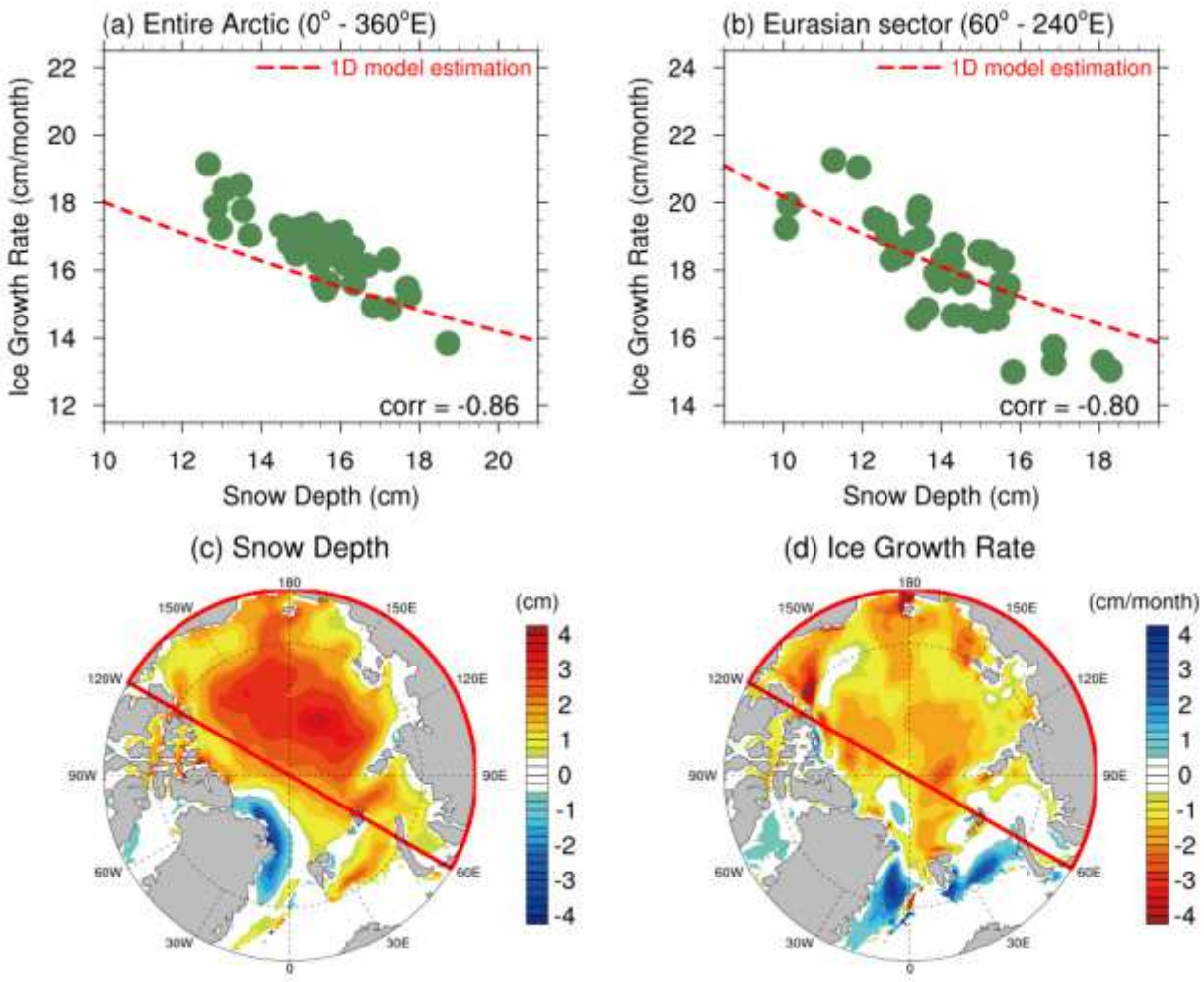

Figure 2

Interannual relationship between snow depth and ice growth.

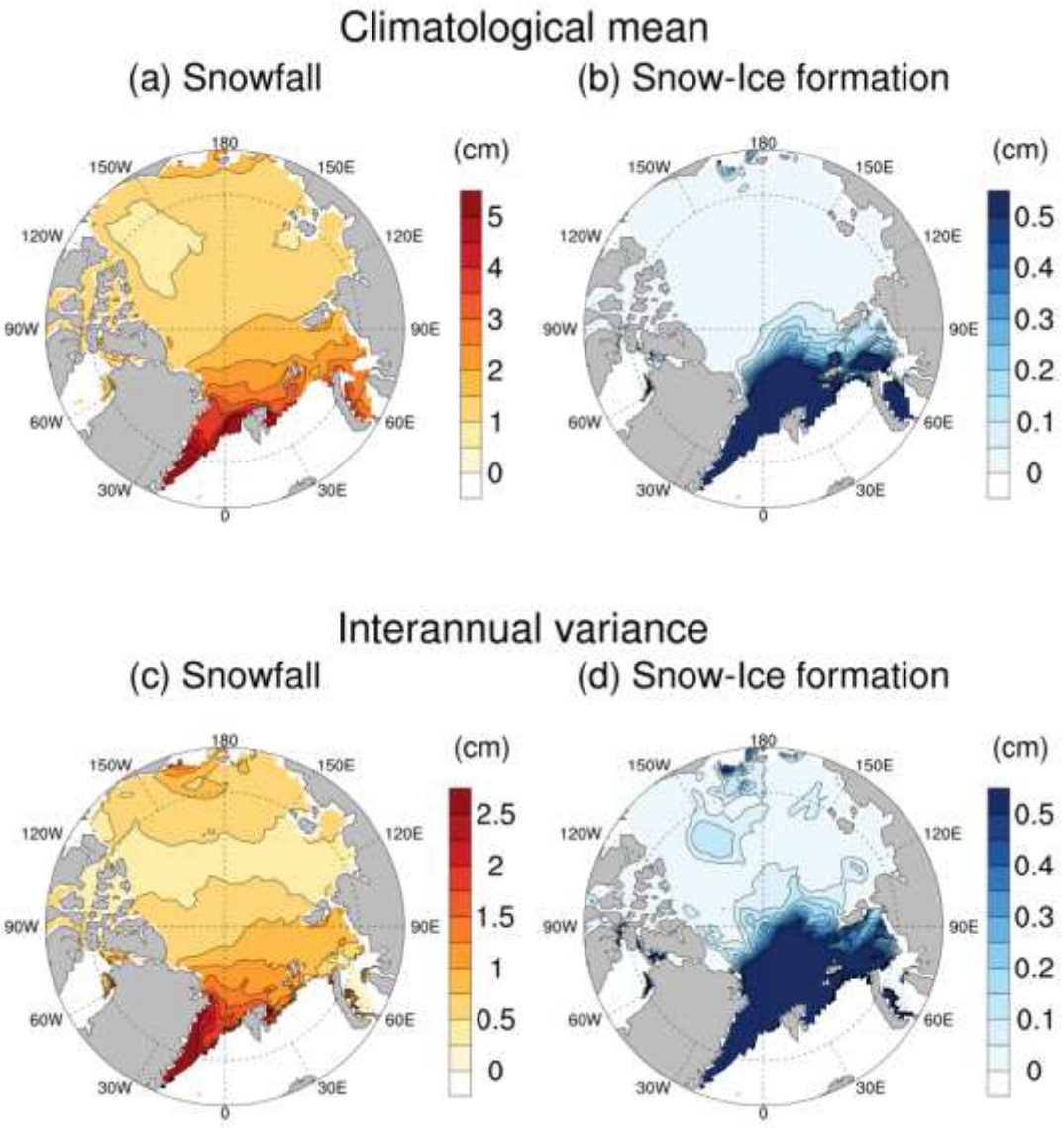

Figure 3

Climatology and variability of snowfall and snow-ice formation

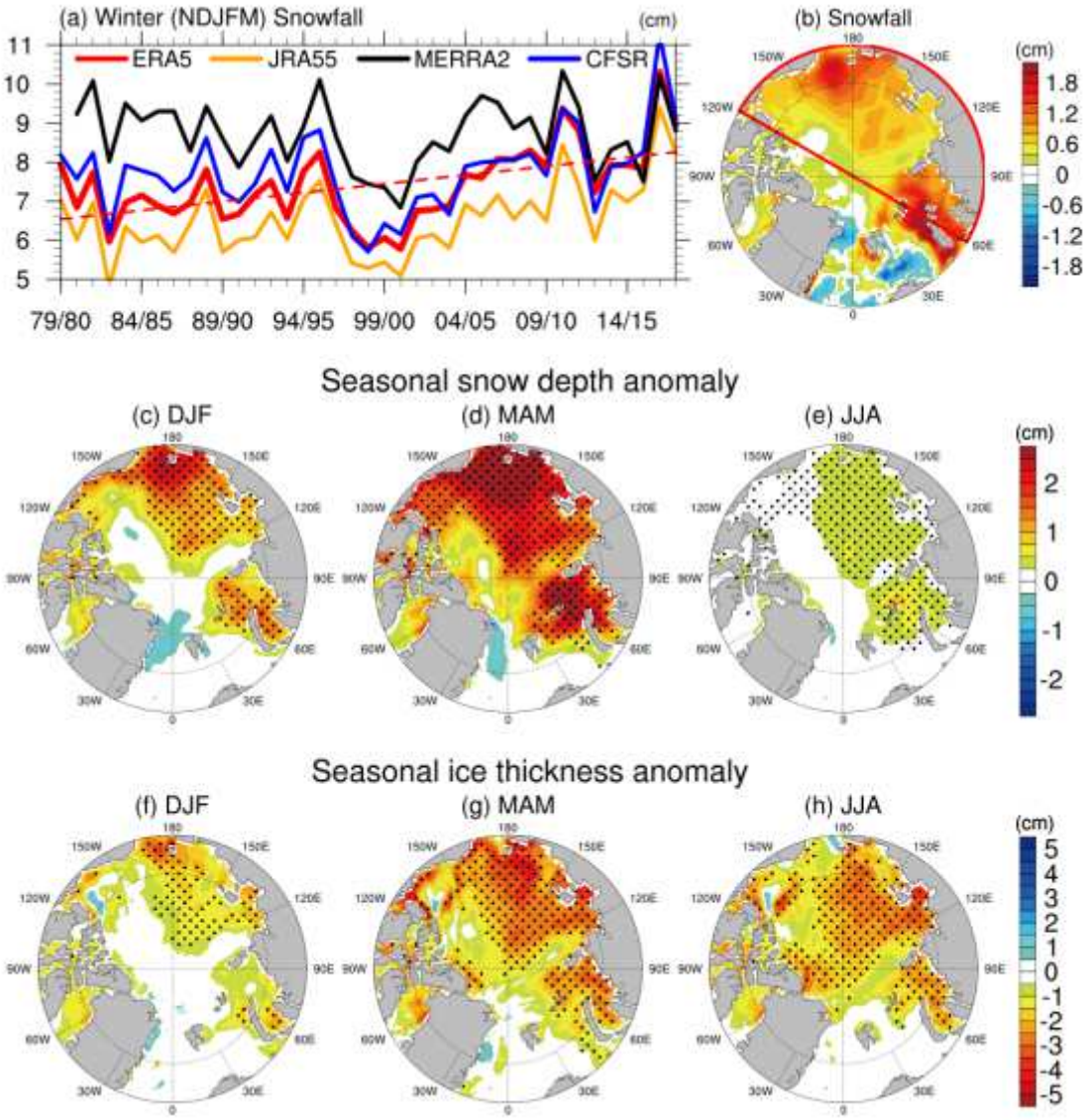

Figure 4

The impact of winter snowfall on seasonal ice thickness

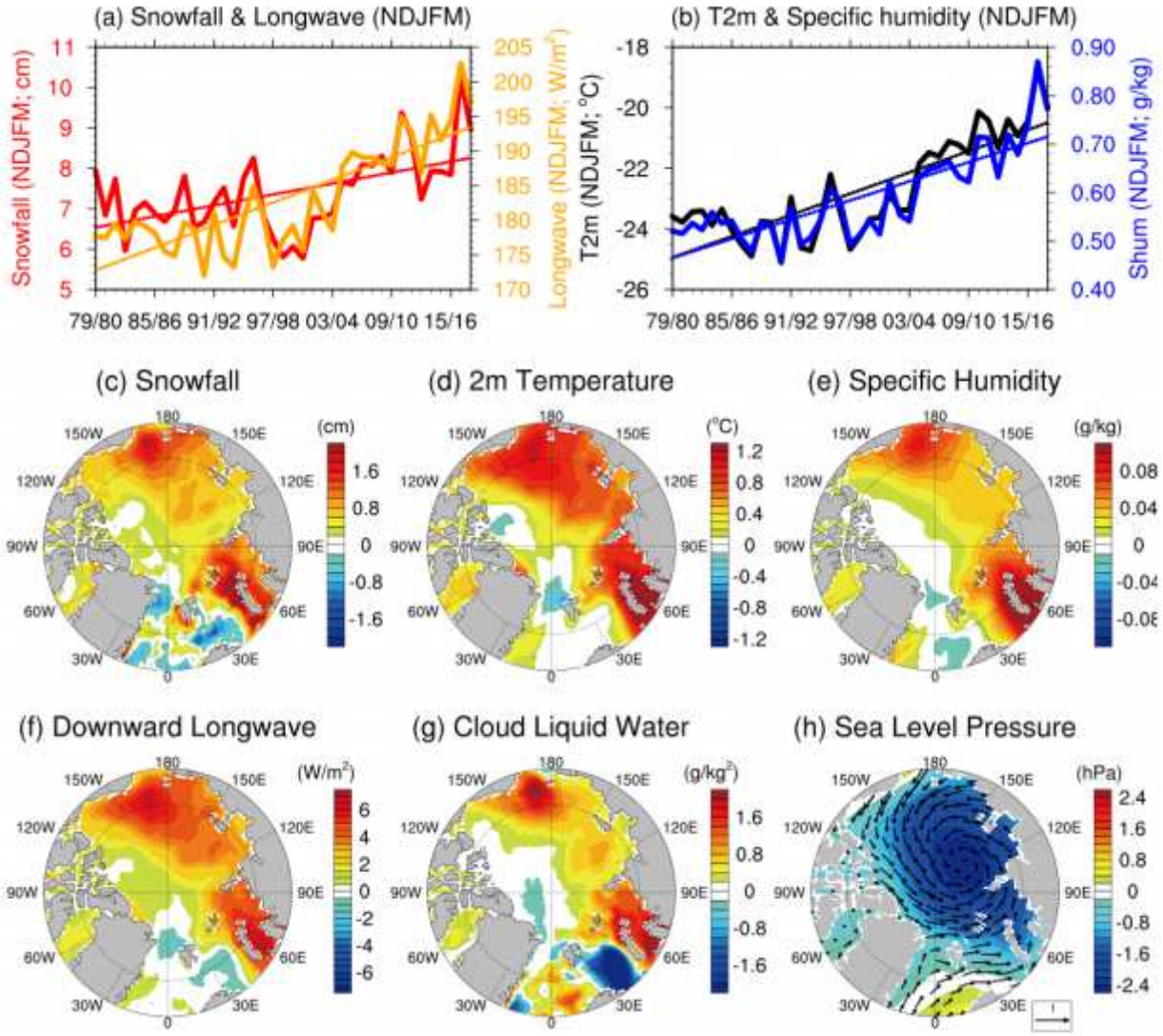

Figure 5

Covariance between winter clouds, snowfall, and downward longwave radiation

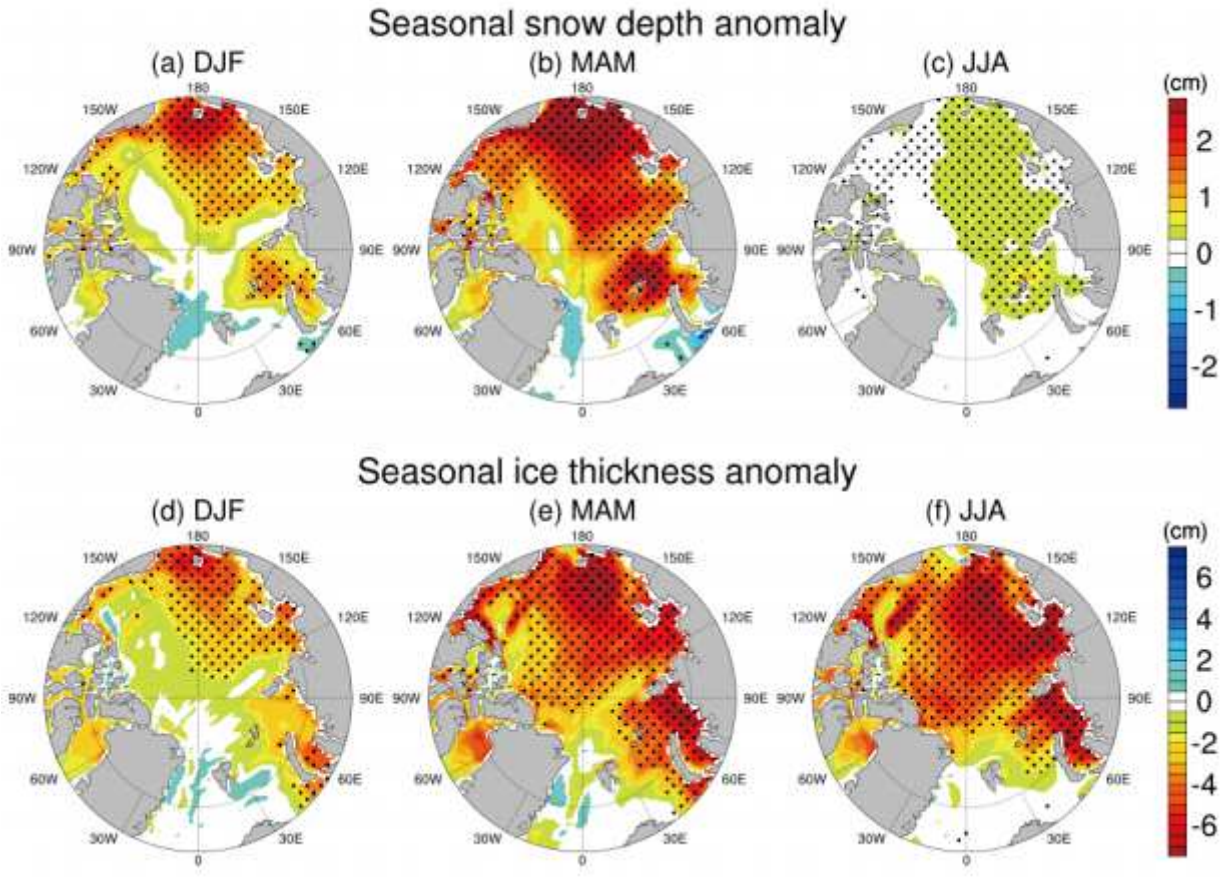

Figure 6

The net effect of the winter snowfall and accompanying atmospheric forcings on sea ice thickness

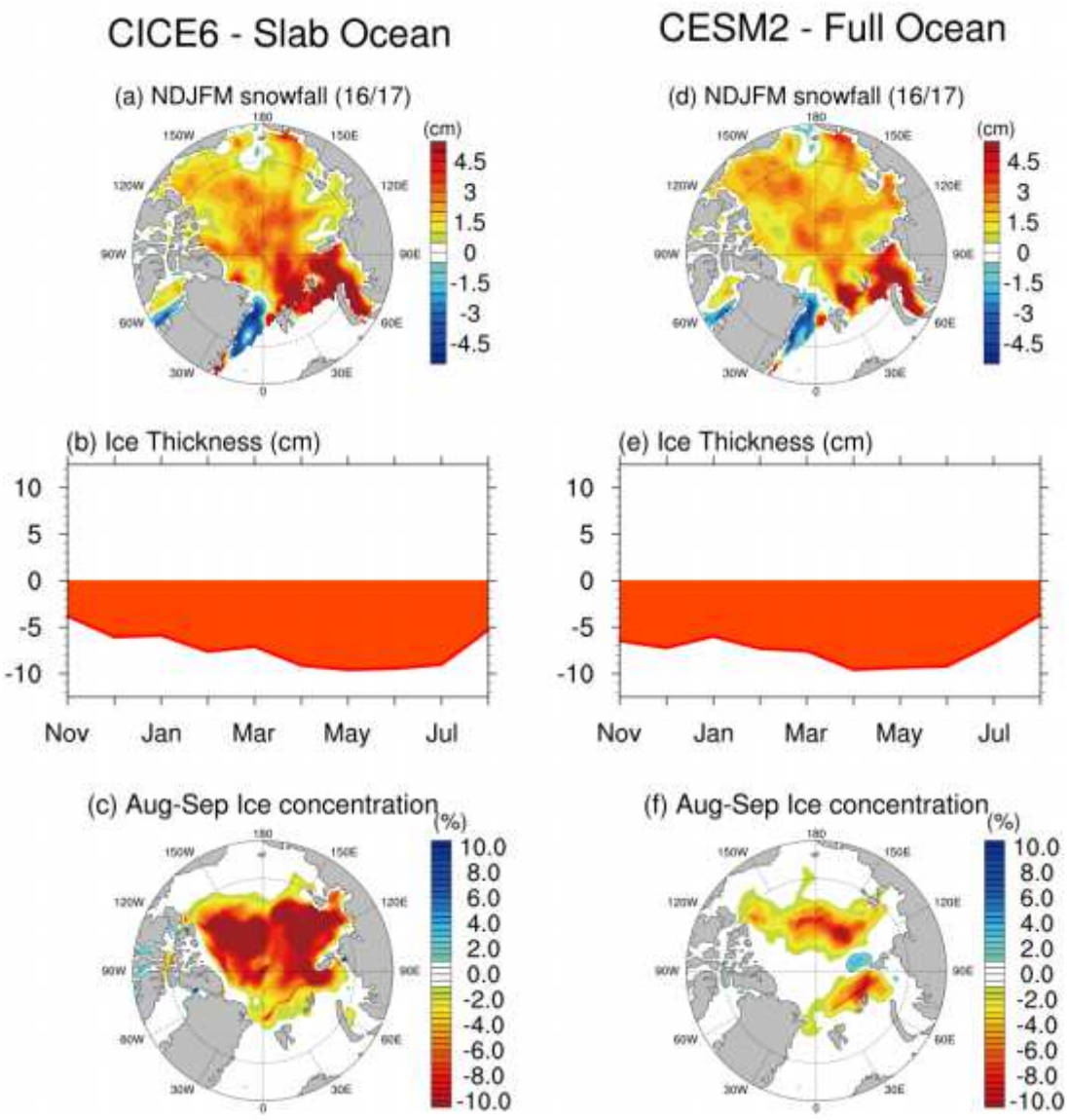

Figure 7

2016–17 sea ice responses simulated by CICE6–slab ocean and CESM2–full ocean models

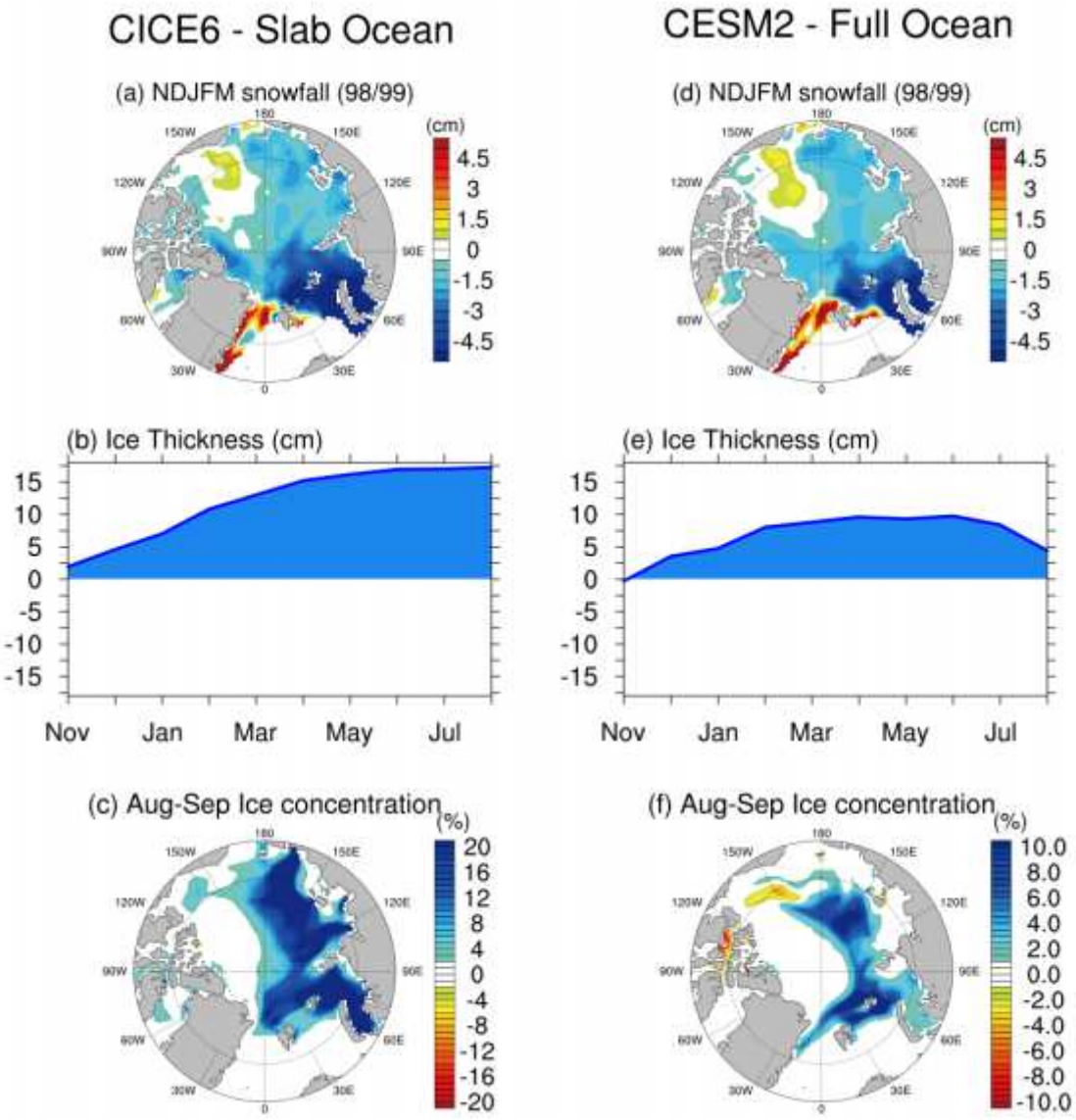

Figure 8

1998–99 sea ice responses simulated by CICE6–slab ocean and CESM2–full ocean models

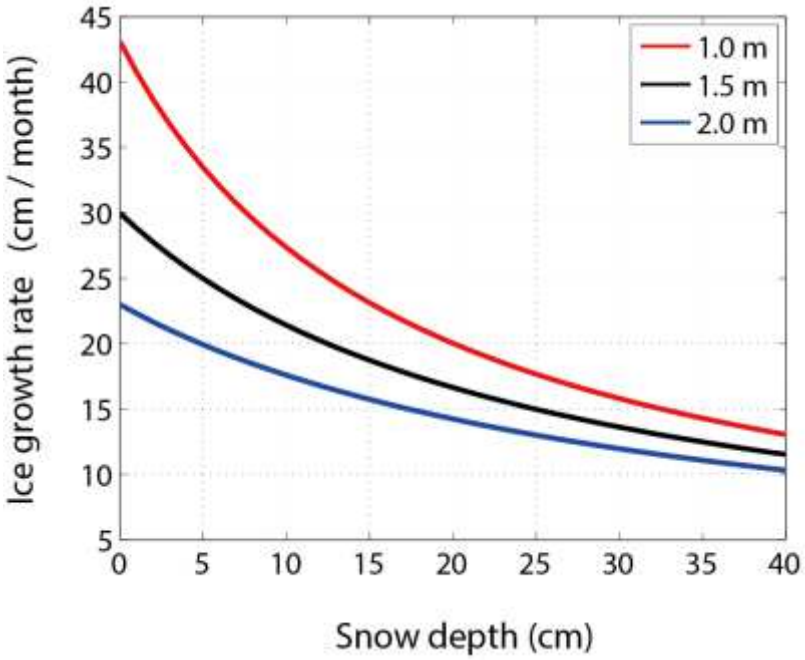

Figure 9

Sensitivity of ice growth rate to snow depth estimated by a simple 1D model

Supplementary Files

This is a list of supplementary files associated with this preprint. Click to download.

- snowCICENCommsSupplv3.pdf